

APPENDIX C

The Linear Decomposition of a Diagnostic
Shelf Circulation Model and Discussion of
Alternate Boundary Condition Formulations

by

J. A. Galt and G. Watabayashi

(Contribution No. 378 from the NOAA/ERL
Pacific Marine Environmental Laboratory.)

September 1978

TABLE OF CONTENTS

	Page
ABSTRACT	453
I. INTRODUCTION	453
II. DECOMPOSITION OF THE DIAGNOSTIC MODEL.	458
III. DENSITY-DRIVEN RESPONSE.	469
IV. WIND-DRIVEN RESPONSE	479
v. MODEL TEST	482
VI. DISCUSSION *	487
VII. CONCLUSIONS.	497
ACKNOWLEDGEMENTS.	500
REFERENCES.	501
TABLE1.	503
FIGURES.	504

The Linear Decomposition of a Diagnostic
Shelf Circulation Model and Discussion of Alternate
Boundary Condition Formulations*

J. A. Galt
Glen Watabayashi

Pacific Marine Environmental Laboratory
Environmental Research Laboratories
National Oceanic and Atmospheric Administration

ABSTRACT. This report will investigate the characteristics of the diagnostic **model** developed at PMEL and documented by Galt (1975) and **Watabayashi** and Galt (1978). The model is partitioned into density driven response and wind driven response components. The density driven response is shown to **consist of the** flow forced by the imposed density field and a minimum **barotropic** mode required to reconcile the density driven flow with the regional **bathymetry**. The wind driven response is associated with **barotropic** currents forced by the set-up of the sea surface across the shelf.

Alternate techniques **used to determine the appropriate boundary conditions** are herein investigated. A formal Green's function for the model equation provides useful insights into regional dynamics and clearly illustrates the dual elliptic and parabolic nature of the formulation. The model solution characteristics are demonstrated on a complex, analytic shelf domain.

I. INTRODUCTION

In this report we will look into the formulation of the boundary conditions and explore certain linear aspects of the diagnostic model equations described **by Galt** (1975). In contrast to past reports on the diagnostic

model (Galt, 1975; Galt, **1976; Watabayashi** and Galt, 1978) that all concentrated on derivations, computer routines, and the study of circulation in a particular **area**, this report will have a more formal approach and will look at the decomposition of the equations into modes. We will discuss the implications of various boundary condition specifications in terms of these modes.

The basic derivation of the *governing* equations of the diagnostic model was **presented** by Galt (1975) and the equations have been described in detail in other places. Using the diagnostic model to study a particular area raises questions that are not directed at the model formulation, but rather at the choice of boundary conditions. The model formulation is a simple combination of **geostrophic** and Ekman modes, but the choice of boundary conditions is complicated by two factors. The first factor is that the **model** equations are second order due to a term which is small compared to the other terms in the dynamic balance. Because of this term, the boundary conditions required to solve the equation come close to overspecifying the flow; spurious solutions are a possible result. Secondly, when the model is used in open ocean regions, further difficulty associated with the boundary conditions results. The flow across the model boundaries is generally unknown, so various approximations are made, and the choice of these then **leads** to potential ambiguities in the solutions. The purpose of this report is to review the various approximations used **to** obtain boundary conditions in the past and to discuss possible **ways of** specifying a less arbitrary formulation for future studies.

Typically, whenever the diagnostic model is applied to a coastal region, one edge of the model lies along the coastline, another edge runs offshore

through deep water, with two lateral boundaries connecting these, from deep water across the shelf to the shore. The **coastal boundary has a strong physical constraint associated with it which makes the formulation of the boundary conditions along the coast relatively easy. Physically, there is no flow through the coast.** Along this coastal boundary four potential modes of flow are allowed: **baroclinic** and **barotropic** geostrophic components, Ekman modes at the surface, caused by wind stress, and at the bottom, caused by frictional drag. Setting the four of these to a net sum of zero involves a mixed Neumann type (**Courant and Hilbert, 1962**) boundary condition. The offshore boundary is typically located in deep water, a region where the classical dynamic height approximations tend to be valid. As a standard, we have simply imposed a dynamic height condition that allows for the flow to be zero at some fixed **level**, typically 1200 meters. To impose this boundary condition, we simply balance the **barotropic** and **baroclinic geostrophic** modes such that **there** is no flow at this depth.

Now we consider **the** two model boundaries which run normal to the coast. When the **model** was initially used, it was assumed that winds along the coast tended to set up the sea surface or push it down across the continental shelf by a mechanism suggested by **Beardsley and Butman (1974)**. By assuming that the sea surface elevation across the shelf was represented by a simple wind dependent hinge, we were able to obtain solutions for the Northeast Gulf of Alaska region (**NEGOA**). The results of these initial studies appeared in the circulation study of the continental shelf off the Copper River Delta, Galt (1976). A moderate refinement on this study was to specify the inflow boundary condition of the flow along the eastern boundary as a simple hinge, adjusting the left hand boundary by hand so that a smoother set of streamlines was obtained along the outflow or western boundary. This was an admittedly

ad hoc approach to the problem, but the result did show some improvement. Galt and Pease (1977) presented flow patterns from this study using this method to simulate drift trajectories for a number of different wind conditions.

When the diagnostic model was applied to the area around Kodiak Island, Alaska, a problem arose with the use of a simple hinge concept. In the Kodiak region the topography is so complex that a simple hinge approach will not reflect the complex circulation **occurring** over the many banks and canyons that cut across the shelf. Hence we made use of the fact that a reduced **inviscid** set of model equations defines characteristics of a first order partial differential equation. These characteristics are very closely related to f/d contours where f is the **Coriolis** parameter and d is the depth. Along these contours the surface elevation is governed by a simple one-dimensional form of the differential equation. Using this method we generated a set of boundary conditions such that the inflow boundary was specified as a simple wind dependent slope, and the outflow boundary was related to the inflow boundary by using the characteristics that were defined by the **simplified** model equations. This approach led to circulation patterns which could then be related to wind conditions. Using this parameterization, a series of different cases was investigated; then the predicted currents from the **model** were **compared** to the scatter seen in current meter records from four different locations in the Kodiak area. The results of these studies were presented at a recent American Geophysical **Union** meeting (Galt, 1977). This characteristic technique was also used in the NEGOA area, and the results of these studies indicated the existence of several distinct domains within the NEGOA area that seemed to be strongly related to each other, (Royer, 1978). A final improvement in the combination hinge and characteristic

technique for determining boundary conditions was the introduction of a sea surface slope inversely proportional to depth to replace the hinge. This modified cross shelf profile meant that steeper sea surface slopes were obtained in shallower water along the coast assuming uniform wind, which tended **to** give a more realistic appearance to the current patterns, these techniques were applied in the Kodiak and NEGOA **regions**.

These techniques were characteristically applied to specific regions to obtain flow patterns for particular studies. They are also all derived in a heuristic way, which is typically labor intensive. The boundary conditions **were** tried; if they did not give reasonable results, alternate formulations were used. Although these empirical studies gave interesting current patterns, and in some cases appeared to accurately reflect direct observations, we still have reason to be skeptical of the results. In **particular, location independent techniques might be derived, reflecting a more solid coupling** of the fundamental physics to the model. Additionally, we are searching for a more formal way to approach the boundary problem as it relates to the diagnostic model.

In the next section we will discuss the decomposition of the model equations into a purely **baroclinic** mode, a minimum **barotropic** mode needed to satisfy continuity, and **a barotropic** wind driven mode. These various modes will be related to the kinds of data needed in order to solve the respective problems and to the number of degrees of freedom that are expected in the solutions. Next, we will discuss the types of boundary conditions to be imposed on each of the separate modes and ways to combine them to give a more general solution that would reflect the given density fields as well as the geometry of the specific region being studied. From these discussions we **will** derive a consistent approach for determining the **boundary**

conditions in a general study area.

In addition we will be able to determine the flow patterns that are likely to result from **these** particular sets of boundary conditions and relate them to observational data that can be obtained from CTD measurements and current meter data. To the extent that observational data do not fit the modal decomposition predicted by the model, we will also derive an objective way of determining whether or not the assumed boundary conditions are correct for the region.

II. Decomposition of the Diagnostic Model

The diagnostic model equations are linear. Therefore it is possible to decompose the governing equations into a number of different parts, each of which can be evaluated individually and then added up to give the **total** solution. The impetus for decomposing the model equations has come **from** two different problems. First of all, the simple hinge type boundary conditions that were used in a number of earlier studies led to a difficulty when the wind velocity approached zero. Under these conditions, the sea surface slope across the shelf also went to zero, thus, there was no **barotropic** transport across these particular boundaries. Nonetheless, the density field which was already specified gave a **baroclinic** transport that could be balanced only by invoking some rather exotic circulation patterns in the bottom Ekman mode. These results clearly indicated that some minimum **barotropic** mode had to exist to satisfy continuity in the presence of a non-uniform density field. A second reason for suggesting a decomposition of the model equations became apparent during an investigation of the number of degrees of freedom to be expected in the general class of solutions. Since the equations are linear, the number of degrees of freedom to be expected must be related to the number of degrees of freedom that are allowed

in specifying the boundary conditions. The **hinge** formulation introduced a single wind parameter; therefore, any similarity type distribution of sea surface elevation across the shelf would always lead to a single pattern in the flow. In order **to** better understand these patterns, **we** broke the boundary conditions into **inhomogeneous** parts related to the density field and a homogeneous and/or similarity part related **to** the set up by the wind. To see that this is possible, we may begin by looking at the diagnostic model equation.

$$N_2 \nabla^2 \xi - J(\xi, d) + N_1 N_2 \nabla^2 \alpha - N_1 J(\alpha, d) - k \cdot \nabla \times \tau = 0$$

where:

ξ = surface elevation, the dependent variable

d = depth

$k \cdot \nabla \times \tau$ = the **curl** of the surface wind stress

N_1 = non-dimensional stratification parameter

N_2 = non-dimensional bottom friction parameter.

A complete derivation of this non-dimensional form of the **vorticity** equation is given by Galt (1975). This can be separated into two parts such that

$$\xi = \xi_1 + \xi_2$$

where these new variables satisfy the following equations:

$$N_2 \nabla^2 \xi_1 - J(\xi_1, d) + N_1 N_2 \nabla^2 \alpha - N_1 J(\alpha, d) = 0$$

which is referred to as the density-driven response

$$N_2 \nabla^2 \xi_2 - J(\xi_2, d) - k \cdot \nabla \times \tau = 0$$

which is referred to as the wind-driven response.

Next we must consider the boundary conditions needed to solve these equations. To do this we will look at a typical model domain consisting of a coastline, shelf and deeper offshore section (see Fig. 1). The various segments of the boundary can be described in the following manner:

Segment a) This **coastline boundary satisfies the physical** condition that the net flux through the coast must be zero. To do this we simply sum the **barotropic, baroclinic**, surface Ekman and bottom Ekman modes in a non-dimensional form (Galt, 1975).

$$-d \frac{\partial \xi}{\partial s} + N_1 \left(\frac{\partial \Delta}{\partial s} + \alpha \frac{\partial d}{\partial s} \right) - \tau_s$$

$$+ N_2 \left(\frac{\partial \xi}{\partial n} - \frac{\partial \xi}{\partial s} \right) + N_1 N_2 \left(\frac{\partial \alpha}{\partial n} - \frac{\partial \alpha}{\partial s} \right) = 0$$

where \bar{n} is a unit vector normal to the coast pointing offshore; and \bar{s} is a unit vector given by $\bar{k} \times \bar{n} = \bar{s}$, where \bar{k} is positive up. These represent mixed Neumann type boundary conditions involving both normal and tangential derivatives of the dependent variable.

Segment b) This offshore or deep water boundary is assumed to be deep enough so that the concepts appropriate to classical dynamic heights can be used. To implement this in the diagnostic model we simply set the sea surface elevation at any station deeper than the level of no motion to:

$$\xi = -N_1 a$$

Segments c & d) These cross shelf boundary regions require special attention. By specifying the surface elevation along this boundary, we supply **Dirichlet** type boundary conditions and determine the **barotropic** flow normal to the boundary. These nonhomogeneous conditions have been approximated in a variety of ways; to understand the rationale behind each potential problem we must look into these in some detail.

Basically the sea surface's departure from a level **surface is caused by both thermohaline forcing and wind forcing. From a conceptual and computational point of view it is useful to separate these into a number of independent cases** or modes. Before doing this, however, it is useful to **outline** the problems that are likely to occur if the boundary values are incorrectly specified.

In the model equation both **geostrophic** and Ekman flow are allowed and must be balanced to maintain continuity of mass. Moreover, around the boundary of the model most of the flow is determined by the independent variables (density, wind stress) or by the boundary conditions. In particular, the density data determines the **baroclinic** component of the **geostrophic flow** through the boundary; and the specification of the sea surface elevation determines the **barotropic** component of the **geostrophic** transport through the boundary. If these do **not balance so that there is no net flow through the boundary**, the model will establish a secondary flow in the bottom Ekman layer to complete the balance. To do this a strong **barotropic** current must **flow** parallel to the boundary. To get a better understanding of how this takes place, we may look at the following simple example (Fig. 2)

Model Domain: (assume y axis pointing North)

$$0 \leq x \leq z$$

$$0 \leq y \leq m$$

$$\text{depth : } d = -\left(2 - \frac{y}{m}\right)$$

$$\text{u-field: } a = ax + by$$

wind field: $\tau = 0$

Substituting these into the governing equation gives:

$$N_2 \nabla^2 \xi + \frac{1}{x} \frac{\partial \xi}{\partial x} = -N_1 \frac{a}{m}$$

Boundary conditions will specify that flow enters from the right and exits from the left of the domain, i.e. ;

$$\begin{aligned} \xi &= y \text{ on } x = 0 & ; & \quad 0 \leq y \leq m \\ x &= l & ; & \quad 0 \leq y \leq m \\ \xi &= 0 \text{ on } 0 \leq x \leq l; & y &= 0 \\ \xi &= y \text{ on } 0 \leq x \leq l; & y &= m \end{aligned}$$

To solve this we will use the homogeneous part of the equation to satisfy the non-homogeneous part of the boundary conditions. Thus

$$\xi = \xi' + \xi''$$

where ξ' satisfies

$$N_2 \nabla^2 \xi' + \frac{1}{m} \frac{\partial \xi'}{\partial x} = 0$$

subject to the boundary conditions given above. The solution for this part of the decomposition is easily seen to be:

$$\xi' = \gamma$$

The remaining part of the solution will satisfy the full non-homogeneous equation subject to the homogeneous boundary conditions, i.e. ;

$$N_2 \nabla^2 \xi'' + \frac{1}{l} \frac{\partial \xi''}{\partial x} = -N \frac{a}{m}$$

$$\xi''(0,y) = \xi''(l,y) = \xi''(x,0) = \xi''(x,m) = 0$$

This differential equation and boundary conditions are well known in the field of oceanography, as they are identical to the one proposed by Stommel

(1948) to represent general ocean circulation. For this secondary **barotropic flow**, the surface elevation contours will also be streamlines for the surface current (Fig. 3). This pattern shows a strong western boundary current analogous to general ocean circulation with the depth gradient taking the place of the β term and the **baroclinic-bottom** interaction term replacing the wind stress curl.

Several general characteristics of the model can be demonstrated from this simplified case. As previously stated the secondary flow is the **result** of a continuity imbalance. The basic **barotropic** mode $\xi' = y$ is nondivergent over the entire domain: The **baroclinic** forcing, on the other hand, is divergent. The density field will induce a flow, with both north and west components, which **carries** water from deep to shallow regions. This requires a secondary flow that results in a southerly drift and/or divergence in the bottom Ekman layer. We can see that this clockwise **flow will** support a bottom Ekman **layer** that transports water out of the domain, primarily through the strong western boundary current region. This strong asymmetry is another general characteristic of the secondary flow generated by the model. The coefficient N_2 is small; as a result, the leading and highest order term typically will not contribute significantly to the balance, except in boundary regions where the derivative in the independent variable can become large (Cole, 1968). For most of the interior and right hand boundary regions (to the right when facing from deep to shallow) the primary balance within the model is between the $J(\xi, d)$ term and the forcing terms. From this we may deduce two additional points. First, as the bottom friction ($\propto N_2$) becomes smaller, the western boundary current becomes more **narrow** and more intense. Secondly, for most of the model domain, the solution is totally dominated by the right hand boundary conditions and first order reduced equation. The intense western boundary current is clearly an artifact

of imposing additional boundary conditions, required by the second order equation, but redundant **to** the dominant first order dynamics. This explains the problem of picking appropriate boundary values across the c and d regions; they are coupled and generally cannot be set independently without expecting to get large, extraneous secondary flows.

With the problem demonstrated, we may now consider several techniques that can be applied in a systematic way to determine appropriate boundary values and define the degrees of freedom, or independent patterns, that can be expected from the model.

We will begin by considering the density driven response in the model, i.e.;

$$N_2 \nabla^2 \xi - J(\xi, d) + N_1 N_2 \nabla^2 \alpha - N_1 J(\alpha, d) = 0$$

To better understand how to proceed we **will** look only at what we know to be the dominant **physics**, i.e., the first order equation that remains when the bottom friction is negligible.

$$J(\xi, d) + N_1 J(\alpha, d) = 0$$

This corresponds to simple **geostrophic** flow over variable **bathymetry**.

Consider a triangular region of the ocean in which the depth, the sea surface elevation, and the vertical integral of the density can be approximated as linear functions of x and y. Thus if we define

$$a = \int_d^0 \rho dz$$

we may write

$a = A_1 \phi_1 + A_2 \phi_2 + A_3 \phi_3$	alpha field
$d = D_1 \phi_1 + D_2 \phi_2 + D_3 \phi_3$	depth
$\xi = Z_1 \phi_1 + Z_2 \phi_2 + Z_3 \phi_3$	surface elevation

where

$$\phi_1 = a_1 x + b_1 y + c_1$$

$$\phi_2 = a_2 x + b_2 y + c_2$$

$$\phi_3 = a_3 x + b_3 y + c_3$$

are the interpolating weight factors or shape functions associated with the triangle in question. (Zienkiewicz, 1971 and Fig. 4). The gradient in the u-field and thus the gradient in the bottom pressure will be:

$$\begin{aligned} \vec{\nabla}\alpha &= \left(\frac{\partial\alpha}{\partial x}\right)\vec{i} + \left(\frac{\partial\alpha}{\partial y}\right)\vec{j} \\ &= (A \cdot a)\vec{i} + (A \cdot b)\vec{j} \end{aligned}$$

Where the indicated three component vectors, A, a and b, are known from the geometry and from the density data given at the vertices. For the moment we will refer to $g\nabla\alpha$ as the baroclinic component of the pressure gradient where g is the acceleration of gravity. Given this assumption, we may define an internal velocity component, or the velocity at the bottom, due to the density variations as

$$\begin{aligned} \vec{v}_I &= \left(-\frac{g}{f\rho} \frac{\partial\alpha}{\partial y}\right)\vec{i} + \left(\frac{g}{f\rho} \frac{\partial\alpha}{\partial x}\right)\vec{j} \\ &= \frac{g}{f} (\vec{k} \times \vec{\nabla}\alpha) \\ &= \left(-\frac{g}{f\rho} (A \cdot b)\right)\vec{i} + \left(\frac{g}{f\rho} (A \cdot a)\right)\vec{j} \end{aligned}$$

This velocity component will be rotated 90° to the left of $\vec{\nabla}\alpha$. We may now look at the depth gradient which can be written as:

$$\begin{aligned}\bar{v}d &= \left(\frac{\partial d}{\partial x}\right)\bar{i} + \left(\frac{\partial d}{\partial y}\right)\bar{j} \\ &= (D \cdot a)\bar{i} + (D \cdot b)\bar{j}\end{aligned}$$

In order to satisfy the continuity requirement that there be no flow through the bottom, we must require that the net horizontal bottom flow be along an isobath. Thus there is a minimum barotropic mode that must accompany the internal velocity V_I unless $\nabla\alpha$ and ∇d are co-linear. This minimal external or barotropic bottom velocity component will be parallel to the depth gradient and be given by (Galt, 1975, eq. 21)

$$\begin{aligned}\bar{V}_{EM} &= -(V_I \cdot \frac{\nabla d}{|\nabla d|}) \frac{\nabla d}{|\nabla d|} \\ &= \frac{f}{\rho} \frac{[(D \cdot a)^2 + (D \cdot b)^2]}{[(A \cdot b)(D \cdot a)^2 - (A \cdot a)(D \cdot b)(D \cdot a)]} \bar{i} \\ &\quad + \frac{[(A \cdot b)(D \cdot a)(D \cdot b) - (A \cdot a)(D \cdot b)^2]}{[(D \cdot a)^2 + (D \cdot b)^2]} \bar{j}\end{aligned}$$

This can be related to the sea surface elevations as follows:

$$\frac{\partial \xi}{\partial x} = \frac{f}{g} (V_{EM})_{\bar{j}} = (z \cdot a)$$

$$\frac{\partial \xi}{\partial y} = \frac{f}{g} (V_{EM})_{\bar{i}} = (z \cdot b)$$

where

$$(z \cdot a) = \frac{1}{\rho} \frac{[(A \cdot b)(D \cdot a)(D \cdot b) - (A \cdot a)(D \cdot b)^2]}{[(D \cdot a)^2 + (D \cdot b)^2]}$$

$$(z \cdot b) = \frac{-1}{\rho} \frac{[(A \cdot b)(D \cdot a)^2 - (A \cdot a)(D \cdot b)(D \cdot a)]}{[(D \cdot a)^2 + (D \cdot b)^2]}$$

and, with no loss of generality, we can set

$$z_1 = 0$$

These three equations can now be solved for the coefficients $Z_1, Z_2,$ and Z_3 to find the minimum barotropic mode.

It can be seen that the minimum barotropic mode is equivalent to specifying the component of the sea surface slope along an isobath, i.e., this determines the barotropic velocity normal to the depth contours. From a graphical viewpoint, the three conditions above are equivalent to placing vertex 1 of the triangle in the x-y plane and then rotating it around the ∇d axis until the slope is sufficient to give V_{EM} (Fig. 4).

Thus far we have determined only one component of the sea surface slope. It is also possible to rotate the solution plane for the sea surface elevation around the axes formed by the isobath. This can be done independently of the rotation around ∇d , physically it will result in a barotropic current that is parallel to the isobath, and thus have no effect on the continuity balance. This degree of freedom can be used to obtain a solution throughout a region composed of a number of triangular elements connected along an isobath or characteristic (Fig. 5). Specifying a slope for triangle 1 is equivalent to specifying the flow along the isobath and the single boundary condition needed to solve the first order partial differential equation. Triangle 2 can be rotated around the isobath until its two common vertices with triangle 1 match up, i.e., the solution plane for triangle 1 and for triangle 2 would be continuous along the common side AB. In a similar manner triangle 3 is rotated around the isobath and matched up along the common side with triangle 2. This process can be carried on through triangles as we follow an isobath or characteristic.

In order to get a better understanding of what is meant by this minimum **barotropic** mode, it is necessary to look into the physical implications of such a **flow**. For's **single** triangle this mode is clearly the **barotropic** component needed to align the bottom **flow** with the **isobaths**. This is an absolute minimum current; any other **barotropic** currents that are consistent with the density field and bathymetry **will** have components of the current **along** the isobath. These other cases would subsequently result **in** a sea surface slope with higher potential energy. When moving from one triangle to another **along** an isobath, continuity of flow across the boundary will determine the along isobath component of flow.

Why should we be interested in a sea surface distribution with minimum potential energy? We may note that this problem was considered by Wunsch (1977) in a different context. He discussed minimum energy solutions subject to a variety of conservation constraints, but none of his constraints happened **to** be bottom flow following f/d contours. He did, **however**, recognize this possibility. To answer the question in the context of the present problem, we **recall** that during the decomposition of the governing equation the density driven response did not include any wind forcing. Under these conditions the wind set up would relax and the sea surface would tend to decrease to the **lowest** energy level consistent with the dynamics represented by this component of the equations.

The next problem is to solve the density response partition of the diagnostic model equations, subject to the constraints that the surface elevation should be at a minimum potential energy and that there are no strong currents generated parallel to the boundary. Following this, we look for solutions to the wind driven response partition of the problem, assuming homogeneous water and some similarity profile for the wind set

up. The linear sum of these two solutions will be the total flow for the diagnostic model problem.

III. Density-Driven Response

The following is an investigation into the density driven response of the model. This will include the **baroclinic** mode and the minimum **barotropic** mode required for continuity. There are several ways to approach this problem, and included are outlines of three of them. Each way represents a somewhat different approach corresponding to various degrees of mathematical rigor. Obviously the computational effort required is quite different for each one of these and a comparison of results is of considerable practical interest.

3.1 Minimum Potential Along Characteristics

The coastal boundary segment previously **labelled** (a) (Fig. 1) must satisfy the "no net flux" condition. The deep water segment (b) will be represented by dynamic heights assuming a level of no motion on the order of 1000 - 1200. The remaining **undetermined** boundary values are for the segments (c) and (d) connecting the offshore and coastal regions. To evaluate these we will make use of the reduced invicid form of equation that represents the dominant physics, i.e.;

$$J(\xi, d) = -N_1 J(\alpha, d)$$

At each boundary point along these segments, the surface elevation is set to an unknown constant c . From this point we will integrate along a characteristic, satisfying the relationship obtained from the above equation:

$$\delta \xi = -N_1 \delta \alpha$$

Once the depth contour, or characteristic, is traced all the way across the model, the initial constant is adjusted to yield the minimum **potential**

energy for the surface profile along that path. A graphical interpretation for each triangle along the isobath is shown in Figure 6. The potential energy along this path can be written as:

$$PE_i = \int_0^{\delta s_i} \int_0^{\xi} \rho g z \, dz ds$$

This gives

$$PE_i = \int_0^{\delta s_i} \frac{1}{2} \rho g \xi^2 \, ds$$

where

$$\xi = (\xi_i + c) \left(\frac{\delta s_i - x}{\delta s_i} \right) + (\xi_{i+1} + c) \frac{x}{\delta s_i}$$

which leads to

$$\begin{aligned} PE_i &= (2\xi_i^2 + \xi_i \xi_{i+1} + 2\xi_{i+1}^2) \cdot \frac{\delta s_i}{6} \\ &+ (4\xi_i + (\xi_i + \xi_{i+1}) + 4\xi_{i+1}) \frac{\delta s_i}{6} c \\ &+ \frac{5}{6} \delta s_i c^2 \end{aligned}$$

Summing these contributions for each of the triangles connected by the isobath with the understanding that $\xi_1 = 0$, gives

$$\begin{aligned} \overline{PE} &= \frac{1}{12} \rho g \sum_{i=1}^{\Sigma} \delta s_i (2\xi_i^2 + \xi_i \xi_{i+1} + 2\xi_{i+1}^2) \\ &+ (4\xi_i + (\xi_{i+1} + \xi_i) + 4\xi_{i+1}) c + 5c^2 \end{aligned}$$

To obtain the minimum value for the potential energy **along** this path we differentiate with respect to c and set the result to zero, giving

$$c = \frac{\sum_{i=1}^n (\xi_{i+1} + \xi_2) \cdot \frac{\delta s_i}{2}}{\sum_{i=1}^n \delta s_i}$$

Once this is done for each of the points along the (c) and (d) boundaries, the interior solution for the full equation should give a minimum potential energy surface except for the contribution from the small bottom stress terms. A closer look, however, reveals several unresolved ambiguities and potentially degenerate cases.

This minimum potential energy approach will give elevations along segments (c) and (d) relative to other members of this set, but it does not suggest how to connect these sections to the offshore segments whose elevations are also only defined relative to other members of their sets. To resolve this **problem we** have adopted the convention that the offshore boundary segment be adjusted up or down by a constant amount so that the innermost line of stations (whose relative position is given by dynamic heights) is at a minimum potential energy relative to the $z = 0$ level. This same constant offset is then applied to the entire deep water region.

The degenerate cases that must be considered involve places along the boundary where neighboring points are at the same depth (characteristic **runs along the boundary**) or where the boundary point is a local maximum or minimum in the depth (characteristic does not penetrate the model domain). We set boundary values at these points by using a quadratic interpolation that fits a curve through two points on one side of the unknown point

and through one point on the other side. This procedure is done from both sides and averaged as shown in Figures 7 and 8.

We summarize this procedure as follows;

- 1) Coastal boundary points are set relative to each other using a "no net flux" constraint.
- 2) Deep water boundary points are set relative to each other by assuming **level** of no motion and using the dynamic heights method. In addition they are offset so that the innermost line of deep stations is also set at a minimum potential energy relative to $z = 0$.
- 3) Cross-shelf boundaries are set relative to each other by minimizing potential energy along characteristics, subject to the reduced form of the density-driven equation.
- 4) Degenerate cases are resolved by using interpolation techniques.

Once these steps have been done, the complete density-driven response is calculated giving a flow field including the effects of bottom friction. This solution can be expected to approximate the minimum potential energy solution (or most relaxed set-up) consistent with continuity considerations, the given density field, and the **bathymetry**.

3.2 Green's Function to Minimize Regional Potential Energy

In this section we will derive a technique for obtaining a complete solution to the minimum potential energy, density-driven response. To do this we will make use of the linearity of the diagnostic model equation.

We start with the general density drive equation:

$$N_2 \nabla^2 \xi - J(\xi, d) + N_1 N_2 \nabla^2 \alpha - N_1 J(\alpha, d) = 0$$

and consider the following series of problems:

1) The solution to the above equation subject to the following boundary

conditions:

- a) no net flux through the coastal segment
 - b) deep **water** boundary segment given by dynamic height and assumed level of no motion plus a constant offset
 - c) **all** of the cross-shelf boundary values set to zero
- 2) The solution to the homogeneous equation is

$$N_2 \nabla^2 \xi - J(\xi, d) = 0$$

subject to the following boundary conditions:

- a) no net flux through the coastal segment
- b) all** remaining boundary points are set equal to zero except one which is given a unit magnitude.

This second problem gives the numerical solution to the Green's function which represents the response of the system to a unit impulse from a particular boundary point. If there is a total of M boundary points along the cross-shelf boundary segments, we repeat problem two above with each point in turn acting as a source point for the Green's function.

In all we obtain **M+1** solutions for each nodal point in the model plus the contribution from the variable density forcing terms with dynamic height values set offshore. After doing this we write the total solution as the linear sum

$$\xi^j = \xi_\rho^j + \sum_{i=0}^M C_i \xi_i^j$$

where the subscript *i* indicates those of Green's functions with which

the solution is associated, the superscript j indicates the nodal point value, and c_j is the 'as yet' undetermined amplitude associated with each of the Green's functions.

We will now determine the values of the c_j 's such that the potential energy for the **total** solution is a minimum. To do this we **will** consider a triangle with vertices $l, m,$ and n and area A . **With** the shape functions $\phi_l, \phi_m,$ and ϕ_n we define the surface elevation as

$$\xi = \xi^l \phi_l + \xi^m \phi_m + \xi^n \phi_n ,$$

The potential energy of the surface relative to a flat surface at zero height (where the integration is over the triangle) is given by

$$\begin{aligned} P &= \int_{dx} \int_{dy} \int_0^{\xi} \rho g z dz dy dx \\ &= \frac{1}{2} \rho g \int_{dx} \int_{dy} \xi^2 dx dy \end{aligned}$$

Substituting our expression for the surface elevation into this gives

$$PE = \frac{1}{2} \rho g \int_{dx} \int_{dy} (\xi^{l2} \phi_l^2 + \xi^{m2} \phi_m^2 + \xi^{n2} \phi_n^2 + 2\xi^l \xi^m \phi_l \phi_m + 2\xi^l \xi^n \phi_l \phi_n + 2\xi^m \xi^n \phi_m \phi_n) dx dy$$

To evaluate the integrals of these shape functions, we may use the formula given by Zienkiewicz (1971, page 120, eq. 7.34) which states

$$\int_{dx} \int_{dy} \phi_1^a \phi_2^b \phi_3^c dx dy = \frac{a!b!c!}{(a+b+c+2)!} 2\Delta$$

and the above integral becomes

$$PE = \frac{1}{12} \rho g (\xi^{l2} + \xi^{m2} + \xi^{n2} + \xi^l \xi^m + \xi^l \xi^n + \xi^m \xi^n) \Delta$$

Substituting our linear sum representation for ξ into the above gives

$$PE = \frac{1}{12} \left[\rho g \left(\xi_\rho^z + \sum_{i=0}^M C_i \xi_i^z \right)^2 + \left(\xi_\rho^m + \sum_{i=0}^M C_i \xi_i^m \right)^2 + \left(\xi_\rho^n + \sum_{i=0}^M C_i \xi_i^n \right)^2 \right. \\ \left. \left(\xi_\rho^z + \sum_{i=0}^M C_i \xi_i^z \right) \left(\xi_\rho^m + \sum_{i=0}^M C_i \xi_i^m \right) + \left(\xi_\rho^z + \sum_{i=0}^M C_i \xi_i^z \right) \left(\xi_\rho^n + \sum_{i=0}^M C_i \xi_i^n \right) \right. \\ \left. \left(\xi_\rho^m + \sum_{i=0}^M C_i \xi_i^m \right) \left(\xi_\rho^n + \sum_{i=0}^M C_i \xi_i^n \right) \right] \Delta$$

Expanding this out gives

$$PE = \frac{1}{12} \rho g \left[\left(\xi_\rho^z \right)^2 + \left(2 \xi_\rho^z \sum_{i=0}^M C_i \xi_i^z \right) + \left(\sum_{i=0}^M \sum_{j=0}^M C_i C_j \xi_i^z \xi_j^z \right) + \left(\xi_\rho^m \right)^2 \right. \\ \left. + \left(2 \xi_\rho^m \sum_{i=0}^M C_i \xi_i^m \right) + \left(\sum_{i=0}^M \sum_{j=0}^M C_i C_j \xi_i^m \xi_j^m \right) + \left(\xi_\rho^n \right)^2 + \left(2 \xi_\rho^n \sum_{i=0}^M C_i \xi_i^n \right) \right. \\ \left. + \left(\sum_{i=0}^M \sum_{j=0}^M C_i C_j \xi_i^n \xi_j^n \right) + \left(\xi_\rho^z \xi_\rho^m \right) + \left(\xi_\rho^z \sum_{i=0}^M C_i \xi_i^m \right) + \left(\xi_\rho^m \sum_{i=0}^M C_i \xi_i^z \right) \right. \\ \left. + \left(\sum_{i=0}^M \sum_{j=0}^M C_i C_j \xi_i^z \xi_j^m \right) + \left(\xi_\rho^z \xi_\rho^n \right) + \left(\xi_\rho^z \sum_{i=0}^M C_i \xi_i^n \right) + \left(\xi_\rho^n \sum_{i=0}^M C_i \xi_i^z \right) \right. \\ \left. + \left(\sum_{i=0}^M \sum_{j=0}^M C_i C_j \xi_i^z \xi_j^n \right) + \left(\xi_\rho^m \xi_\rho^n \right) + \left(\xi_\rho^m \sum_{i=0}^M C_i \xi_i^n \right) + \left(\xi_\rho^n \sum_{i=0}^M C_i \xi_i^m \right) \right. \\ \left. + \left(\sum_{i=0}^M \sum_{j=0}^M C_i C_j \xi_i^m \xi_j^n \right) \right] \Delta$$

This is once again the potential energy associated with a single triangle as a function of the Green's function contribution from each boundary point along the cross-shelf segment. The total potential energy for the

region will be the sum of this expression over each triangle. To minimize this we must differentiate with respect to each of the C's and set the resulting system of equations to zero, i.e., for $i = 0, 1, 2, \dots, M$

$$\Delta \left[2\varepsilon_p^l \varepsilon_i^l + 2\varepsilon_p^m \varepsilon_i^m + 2\varepsilon_p^n \varepsilon_i^n + \varepsilon_p^l \varepsilon_i^m + \varepsilon_p^m \varepsilon_i^l + \varepsilon_p^l \varepsilon_i^n + \varepsilon_p^n \varepsilon_i^l + \varepsilon_p^m \varepsilon_i^n \right. \\ \left. + \varepsilon_p^n \varepsilon_i^m + 2\varepsilon_i^l \left(\sum_{j=0}^M \varepsilon_j^l C_j \right) + 2\varepsilon_i^m \left(\sum_{j=0}^M \varepsilon_j^m C_j \right) + 2\varepsilon_i^n \left(\sum_{j=0}^M \varepsilon_j^n C_j \right) \right. \\ \left. + \varepsilon_i^l \left(\sum_{j=0}^M \varepsilon_j^m C_j \right) + \varepsilon_i^m \left(\sum_{j=0}^M \varepsilon_j^l C_j \right) + \varepsilon_i^l \left(\sum_{j=0}^M \varepsilon_j^n C_j \right) + \varepsilon_i^n \left(\sum_{j=0}^M \varepsilon_j^l C_j \right) \right. \\ \left. + \varepsilon_i^m \left(\sum_{j=0}^M \varepsilon_j^n C_j \right) + \varepsilon_i^n \left(\sum_{j=0}^M \varepsilon_j^m C_j \right) \right] = 0$$

This gives $M+1$ equations in the $M+1$ unknown C's, which can be written in the matrix form.

$$A \mathbf{c} = \mathbf{\Gamma}$$

Where

$$\Gamma_i = -[(\varepsilon_p^l + \varepsilon_p^m + \varepsilon_p^n)(\varepsilon_i^l + \varepsilon_i^m + \varepsilon_i^n) \\ + (\varepsilon_p^l \varepsilon_i^l + \varepsilon_p^m \varepsilon_i^m + \varepsilon_p^n \varepsilon_i^n)] \Delta$$

And

$$A_{ij} = [(\varepsilon_i^l + \varepsilon_i^m + \varepsilon_i^n)(\varepsilon_j^l + \varepsilon_j^m + \varepsilon_j^n) \\ + (\varepsilon_i^l \varepsilon_j^l + \varepsilon_i^m \varepsilon_j^m + \varepsilon_i^n \varepsilon_j^n)] \Delta$$

and where it is understood that these terms are summed over **all** the triangles,

Solving this system for the C_z 's, we then obtain the minimum potential energy solution for the density-driven response partition of the diagnostic model.

3.3 Natural boundary conditions for the Finite Element Solution

The third method of estimating the boundary conditions for the **density-driven** response to the model is by far the simplest and depends to some extent on serendipity. The basic procedure can be described as follows:

The density-driven response partition of the diagnostic equation is **solved** using the finite element technique and first-order linear shape functions subject to the following conditions:

- a) **Along the coastal boundary segment a zero net flux condition is specified**
- b) **Along the deep water boundary segment the elevations are set using dynamic height considerations**
- c) **Along the cross-shelf boundaries no boundary conditions are imposed after the finite element matrix is assembled.**

Surprisingly, a solution is then obtained without giving the elliptic problem explicit boundary conditions surrounding the domain. Furthermore, the resulting flow pattern appears to be very close to the one that was obtained using the technique of minimizing the potential energy along a characteristic or using the more complete Green's function minimization. To understand how this takes place we must first consider the finite element **(FEM)** method that is being used along with its bases set of functions. Next we will investigate the physical implications of these mathematical conditions and discuss why these should lead to a low or minimum potential energy state.

We start by observing that the differential operator represented by the diagnostic model equation is second order; we therefore expect the solution to come from the general function space of twice-differentiable functions. On the other hand, the interpolation functions which are used to make up the solution function space are only linear and piecewise continuous. This presents no particular problem in that the actual Galarkin formulation that is used to assemble the FEM solution matrix is in the "weak form" where higher derivatives in the operator are transformed to boundary constraints via integration by parts. When this is done, certain essential and natural type boundary conditions are identified (Strang and Fix, 1973). In the absence of the specification of essential boundary conditions (Dirichlet in this case) the solution will tend to optimize its approach to the natural boundary conditions (homogeneous Neumann type). In essence, when no boundary conditions are specified over some segment of the boundary, the normal derivative of the FE solution using first-order elements and the weak Galarkin form will tend to go to zero.

The sea surface slope normal to the boundary of the model corresponds to a barotropic flow along the edge of the domain. This type of circulation pattern has been previously identified as resulting from continuity mismatches around the boundary. It is at least plausible that by approaching natural type boundary conditions along the boundary segments crossing the shelf, the secondary flows will be small in some sense. Thus we can expect the total solution, constrained with essential conditions only around the deep water segment and the physically realistic non-flux conditions along the coast to approach a minimum energy state.

In this section we have presented three different approaches to solving the density driven response to the diagnostic model equations. Each rep-

resents a somewhat different point of view and requires different amounts of computational effort. These are investigated in section V to add formalism to the understanding of the model and to standardize the approach to its use. This is in strong contrast to previous explorations where trial and error and oceanographic intuition were major factors in model applications.

IV. Wind-Driven Response

In this section the wind-driven response of the model is considered by solving the partition of the diagnostic equation given by

$$N_2 \nabla^2 \xi - J(\xi, d) - k \cdot \nabla \chi \tau = 0$$

This equation represents the wind forcing of the model region. The wind-driven effects can be conveniently divided into two separate components. The first of these is the surface Ekman flow, which enters into the vorticity equation as the curl of the wind stress (i.e., the local wind forcing caused by the winds within the model region.) The second category of wind forcing can be referred to as global. This is the result of large-scale wind patterns and is transmitted to the model through the set-up of the boundary points. Typical patterns associated with this process are modeled by imposing a slope across the continental shelf region that is proportional to the alongshore component of the wind stress. The assumed mechanism hypothesizes that the Ekman transport pushes water up against the coast inducing a barotropic set-up and subsequent alongshore currents. Such behavior has been qualitatively observed in many continental shelf areas and quantitatively documented by Beardsley and Butman (1974).

Looking more closely at the local wind forcing, we find that there are two ways in which the model can be forced directly by winds within

the model domain. The first of these **is through** the wind stress curl, which is small for typical length and time scales (100 km and days). For most cases, the open ocean, wind-driven convergence or divergence is a secondary contributor to the mass balance, or sea surface set-up. The second way that the local winds drive the model is through the mass convergence or divergence at **the coastline**. This effect enters through the **no net flux boundary conditions**. This direct forcing of the model covers all possible ways in which winds effect the dependent variable, i.e., sea surface elevation and subsequently the **geostrophic** currents at the surface. However, these effects do not include all of the wind-driven currents. Superimposed on this surface **geostrophic** current is the non-divergent component of the Ekman layer flow which is added onto the diagnostic **model** solution and clearly depends on local winds.

The global **wind** forcing to be used in the **model** presents two distinct problems. The first is theoretical, the second numerical. It is known that regional winds set up the sea surface. The details of how the physical processes operate in continental shelf regions with complex bathymetry and stratification are essentially unknown. **Because of this, various assumptions** have been made and tested with the model. The measure of success of these assumptions is a comparison of model results **to** current meter observations or Lagrangian drifter data. To date, only the simplest one parameter similarity profiles have been used, specifying either a uniform slope across the shelf or a slope inversely proportional to the depth. **In** these cases using the complete model, the density-driven and wind set-up effects were not clearly separated, and it was difficult to determine the actual degrees of freedom represented by the **model** or specified in the boundary formulation. The natural way to specify these

wind-driven elevation values across the shelf would be to have sea surface or bottom" pressure measurements from a series of gages. Using this data, an observed cross-shelf profile could be used to drive the model. The **pressure data would** need to be filtered to remove **non-geostrophic** components. In addition it would be encouraging to find the appropriate **geostrophic** scale signal falling along a simple one-parameter cross-shelf profile.

When trying to key the wind-driven model response **to** various **cross-shelf** profiles, it is important to remember that the system is linear. For example, with **n data points** across the shelf, **n** different **empirical** orthogonal modes can be derived **from** the records. Then all possible profiles can be represented as linear combinations of these few model profiles. Thus, these studies can expect the most productive output by concentrating on empirically derived profiles.

An alternate technique for keying the wind-driven response of the **model** would be to develop a Green's function for various slope conditions between nodal points across the shelf. Methods would be similar to those presented in the preceding chapter and could be put together in linear combinations to represent any given cross-shelf profile.

The second general problem associated with the **global** wind forcing in the model is numerical and was **discussed** in section III of this report. As mentioned, the boundary layer nature of the governing equation and the dominant first-order physics associated with the bathymetric interaction term make it essential to consider the coupling between the right-hand and left-hand cross-shelf boundary segments. The two opposite boundary values must be related along bathymetric contours to avoid the presence of extraneous boundary currents in the secondary flow. There are several possible approaches to this problem; as discussed previously. The first

approach is to specify the surface elevation at only one point on each isobath and determine the second boundary value by using the reduced equation and integrating along the characteristic. The second approach makes use of the natural boundary condition behavior of the finite element solution technique. In this case, the elevation would be set on each characteristic and the remaining boundary conditions would remain unspecified to be determined by the solution technique so as to suppress extraneous boundary currents.

As a final point on the wind-driven response in the model, this partition of the model equation does not depend in any way on the density data. The initial finite element grid or nodal point positions were determined by the locations of CTD stations which supplied the density input. Commonly **ship time and weather constraints limit the station coverage, and spatial distribution is not as detailed as one might like for resolving complex** bathymetry. With the density- and wind-driven responses of the model partitioned as indicated, it is not necessary to restrict both partitions to the same finite element mesh. In fact, the wind driven response can be run once for any region on a grid as dense as needed to resolve the relevant topographic features.

V. Model Test

In order to get a better understanding of the model decomposition the model was tested on a relatively complex domain. Rather than go to a specific site and attempt to find data, a region was hypothesized with analytic bathymetry. The topographic features of the region are: a broad continental shelf, a bank or shoal region on the shelf, and a **large** submarine canyon. The actual model bathymetry is the sum of **all** these features

expressed in analytical non-dimensional form as follows:

$$d(x,y) = D_0 - \frac{1}{(D_2 + \exp(D_3 y^2))} + D_{11} \frac{(Y-Y_2)}{(Y_3-Y_2)} \\ + D_4 \exp(-D_5(x-x_0)^2 - D_6(y-y_0)^2) \\ + D_9 \exp(-D_7(y-y_1)^2 - D_{10}(x-x_1)^2) (1 - \exp(D_{12} y^4) \cos(D_8(x-x_1)))$$

Figure 9 shows the triangular grid system that was used on the 5 x 5 (non-dimensional units) domain. This corresponds to 143 stations with an increased density of points on the western boundary to avoid any resolution problems that might occur with the **secondary boundary currents**. **Figure 10** shows a bathymetric contour map plotted from the station location data. We will refer to this as the **GS (Gondwanaland Shelf) domain**.

The density field will be given by a simple linear function of position at the surface that goes to a constant density at great depth, i.e.,

$$\rho = \rho_0 - (\delta\rho_1 x + \delta\rho_2 y + \delta\rho_3) \exp(D_{13} z)$$

This can be easily integrated from some depth z to the surface to give α , i.e.,

$$\alpha = \int_z^0 \rho dz = -\rho_0 z - \frac{(\delta\rho_1 x + \delta\rho_2 y + \delta\rho_3)}{D_{13}} (1 - \exp(D_{13} z))$$

From this the gradients in the α field and bottom pressure forces due to the **baroclinic terms** will be

$$\frac{\partial \alpha}{\partial x} = - \frac{\delta\rho_1}{D_{13}} (1 - \exp(D_{13} z))$$

$$\frac{\partial \alpha}{\partial y} = - \frac{\delta\rho_2}{D_{13}} (1 - \exp(D_{13} z))$$

Table 1 gives the non-dimensional values of the various depth and density coefficients used in the GS region parametrization. This relatively **simple formulation retains analytic properties yet requires some CROSS-isobath** flow in the minimum **barotropic mode**; thus it will be an informative example for the present study. Figure 11 shows the alpha field derivations plotted from the station data.

To round out the Gondwannal and Shelf domain data set, it is assumed that a number of pressure gages and meteorological data buoys have been deployed and have established the wind response characteristics of the region. For the present example this has reduced to the following: the sea surface elevation for any point along the coast (corrected for tide and barometric pressure) **is** a linear function of the alongshore component of the wind stress with the **amplitude** of the variation being roughly proportional to the width of the shelf. Then, for the purpose of this illustration, a linear bathystrophic forcing is hypothesized. In this the **alongshore** component of the flow is proportional to the alongshore component of the wind speed with the onshore/offshore component of the sea surface elevation in **geostrophic** balance with the alongshore current.

Given this GS domain **data, we may now explore the regional** circulation using the decomposition techniques outlined in the previous two sections of this report.

Starting with the density-driven response we will seek the **baroclinic** mode along with the minimum **barotropic** mode required for continuity. Three different methods of solution are suggested, and each will be investigated. The assumed level of no motion offshore will be taken as 1,000 m, thus the two outermost lines of stations will be set using dynamic height considerations.

The **three methods are:**

1) To obtain the boundary values using the minimization of potential energy along characteristics we proceed as outlined earlier. The surface elevation associated with the minimum **barotropic** mode for this case is shown in **Figure 12a**.

2) To solve for the density-driven flow using the Green's function approach we must calculate a number of different components to the flow. The first is the component forced by the offshore dynamic heights. This solution is shown in **Figure 13a** and can be thought of as the basic **baroclinic** forcing. Added to this will be a linear combination of the other Green's functions components. The first will be the constant elevation for the offshore region which corresponds to offshore adjustment necessary to minimize this region relative to the $z = 0$ level. This is shown in **Figure 13b**. The other Green's function components are all related to a unit displacement at some boundary point. An example is given in **Figure 13c**. Following the techniques outlined previously, the appropriate Green's function components are scaled and added to minimize the potential energy of the solution. The resulting surface elevation for the minimum **barotropic** mode is shown in **Figure 12b**.

3) The third technique for estimating the minimum **barotropic** mode is to use the finite element natural boundary condition formulation. **Figure 12c** shows the surface elevation predicted by the natural boundary condition case.

Figure 14 shows the surface velocity for the same three cases as seen in **Figure 12**. **Figure 15** shows the corresponding bottom velocities for the three techniques. This differs from the surface currents by the

baroclinic shear that is introduced by the variable density.

We now turn our attention to the wind-driven response of our GS region. As previously stated, the assumed input data suggests a bathystrophic balance where the alongshore component of the wind is linearly related to a uniform sea surface slope across the shelf. This determines the boundary conditions that we will impose on the wind-driven component of the model decomposition.

Before considering the details of how to apply these conditions, we note that the wind-driven response does not depend in any way on the density data so that alternate grid systems are possible. To take advantage of this we will add stations in regions of particular interest for increased resolution of key bathymetric features. These additional stations will be added over the canyon, the shelf break and the shoal area. The more detailed grid system and new triangle mesh are shown in Figure 16.

The wind set-up forcing requires a uniform slope across the shelf of the GS domain. This forcing applied to any cross shelf section can be represented by a linear hinge. We set these with a slope of unity between the 1,000 m (non-dimensional depth 5) contour and the coast. In addition to these Dirichlet conditions we will assume the winds do not affect the deep offshore region so these values will be set to a constant equal to the value of the offshore extreme of the right-hand boundary. The coastal boundary segment will be subject to the usual "zero net flux" conditions. The complete wind set-up solution will be the linear sum of these forced hinge sections, each of which can be thought of as the Green's function response of the domain to an imposed bathystrophic balance across a particular shelf profile. For each of these hinge components,

the cross-shelf profile will be set; remaining cross-shelf model boundaries will be subject to the FEM natural boundary conditions.

The key question is; along which cross-shelf profile **should** the hinges be set? Where the bathymetric constraints dominate, either side should lead to the same result. On the **flat** nearshore segments of the **shelf**, however, the length scale is still determined by the elliptic terms in the equation and the influence of boundary values (or forced hinge) fall off with distance like the Green's function components. To explore these options three **barotropic** cases are run with the surface elevations shown in Figure 17 and the current vectors shown in Figure 18.

For each of these, alternate cross-shelf profiles would lead to alternate possible circulation patterns with the total number of degrees of freedom corresponding to the number of degrees of freedom in the specification of all of the cross-shelf profiles.

VI. Discussion

The **GS** numerical experiments can now be discussed, comparing first the density-driven response and the three different techniques that have been used to find the minimum **barotropic** mode. As discussed in section two of this report, a minimum **barotropic** mode is required because the given density distribution we have chosen is quite simple and the bathymetry is no more complex than that which might be expected of a typical shelf region, the joint interaction between these two fields becomes relatively complex. It is useful to examine the deviations in the alpha **field** along the bottom (Figure 11). Clearly the major bathymetric features and density field result in a complex pattern in the bottom pressure, or more specifically the lateral bottom pressure gradients. The details of how these interactions

effect the flow are represented as a $J(\alpha, d)$ torque term in the differential equation; this pattern of $J(\alpha, d)$ is shown in Figure 19. The resulting flow must satisfy both kinematic continuity constraints and conservation of vorticity conditions. The divergence in the flow (vertical stretching as the water moves over sloping bathymetry) interacts with the planetary vorticity and results in the development of shears and horizontal accelerations. In addition to these constraints, which are defined and controlled by the differential equation in the interior, we impose the boundary conditions that specify the form of the solution around the edge of the model. Our basic premise is that in the absence of wind set-up the sea surface should be at a low potential energy state, or that the flow's interaction with the bathymetry should be in some sense small; and that the solution should not show any strong or irregular currents along the open boundary regions across the shelf. Each of the three techniques used to obtain boundary conditions concentrate on obtaining low potential energy solutions overall, or on forcing a smooth boundary region. The general features of the flow can be seen in Figures 12, 14 and 15.

Looking first at minimizing the potential energy along reduced characteristics (Figures 12a, 14a and 15a) the general features of the density-driven flow are clear: 1) In general the flow is weak and energetic current bands do not develop, which is consistent with our initial premise. 2) As the forced onshore flow first encounters the steep continental shelf the baroclinic/bathymetric interaction term introduces a general turn to the east in the surface currents, with the bottom flow moving slowly to the original westward direction, paralleling the isobaths. 3) Over the shoal area on the eastern segment of the shelf a counterclockwise

circulation develops with intensified flow over the eastern slope of this positive bathymetric feature. 4) Over the canyon that cuts through the western segment of the shelf a clockwise circulation is observed, with the more intense currents found over the western slope of this negative bathymetric feature. 5) Along the shallow relatively **flat** coastal segment of the shelf region the flow is weak and generally to the east. Finally, 6) the offshore level of no motion and continental slope interaction region exhibits what appears to be a banded east-west current pattern that is particularly evident along the smooth eastern segment of the slope region. The bottom flow predicted by this approach is generally **small** (virtually zero over most of the shelf) and along isobaths, with the exception of a few boundary triangles right in the steepest region of the continental slope where the water that is forced onto the slope must exit the model. This is obviously an open boundary effect that the characteristic approach was not able to totally suppress.

We may now turn our attention to the more rigorous Green's function minimization of the potential energy. The results of this case study can be seen in Figures 12b, 14b and 15b. The numerical technique was verified to have actually obtained an overall minimum potential energy sea surface and the potential energy was found to be a quadratic function of the component amplitudes, as expected. The potential energy of the characteristic technique was 40% greater than the Green's function method. The general behavior of the solution can be discovered by looking at the individual components shown in Figure 13. Figure 13a is the basic **baroclinic** forcing and clearly shows that the interior is going to have **baroclinic** circulation associated with both the canyon and shoal regions. In addition a weak coastal current and the effects of the sharp discontinuity between

the offshore and interior region are evident. Figure 13b shows the **barotropic model response associated with the elevation offset** between the offshore **and** interior region. **The** major flow is along the continental **slope**, but the flow is also seen to extend into the canyon region and across **isobaths**, particularly in the shallow shelf region where the bottom friction plays a significant role. It is obvious that this can be combined with the **baroclinic** forcing (shown in Fig. 13a) in such a way as **to largely** cancel out the strong currents along the continental slope. Also pertinent to this Green's function component **is** the significant boundary layer that occurs on the western edge of **the** model. This is due to **the** cross-isobath flow that takes place gradually throughout the interior of the model and must be compensated for in the narrow return flow. Actually this is just a more complicated example of the flow which is described in section II and shown in Figure 3. The remaining Green's functions all show the model's **barotropic** response to elevation at a single boundary point (Fig. 13c). In the absence of strong bathymetry, the response is controlled by the elliptic terms in the model equation, and bottom friction sets the length scale.

In Figure 14b we see that the composite Green's function currents exhibit **all** of the six features of the interior flow that were enumerated for the results of the reduced characteristic technique. There are **essen-**
tially no differences in the surface current vectors except in the western boundary region of the model where significant boundary layers are present. The bottom currents from the Green's function solution are uniformly very small except in the boundary region where some are surprisingly large. This approach clearly does not handle all of the extraneous boundary layers that occur, and some additional research would seem appropriate.

In **re-examining** the total potential energy of the model we may note that very strong boundary currents are possible with relatively minor potential energy changes in the small boundary triangles. In addition, when the large interior regions are included in the minimization, a very slight change over this area (representing a large potential energy) may balance a relatively extreme perturbation along the edge. At this point we should also invoke some of our fundamental understanding of how partial differential equations are solved and of the significance of boundary conditions in the construction of solutions. Basically the differential equation must specify the nature of the solution within the interior of the domain. Along the boundaries the nature of the solution must be imposed, and for these regions this is typically more significant than the control exerted by the differential equation. This **all** suggests that to minimize the potential energy over the entire model may be an incorrect strategy. It tends to specify the solution too rigidly over the interior and doesn't properly force the correct form of the solution in the critical boundary regions.

We can now examine the results of using the natural boundary condition technique shown in Figures **(12c, 14c and 15c)**. The surface contour **pattern** appears to be very close to the one obtained by the characteristic and reduced equation technique. The six major features described in the previous cases are essentially unchanged by this technique.

Two interesting features do show up in the natural boundary condition case that were not seen in the characteristic or complete potential energy minimization/Green's function cases. First of all, there is no evidence of enhanced boundary currents. The total potential energy is 28% greater than for the Green's function minimization. This appears as a slight

offset over the interior with a much smoother surface **in the** boundary regions.

The second major feature of the natural boundary condition solution is that the bottom currents (Figure 15c) are zero, unlike the other cases. In this respect the solution appears to be a direct extension of the offshore dynamic heights methods adjusting the **level** of no motion to the **bathymetry**. Looking back at the basic differential equation it is clear that zero bottom currents (i.e., $\xi = -N_1\alpha$) $\xi^* = (\xi + N_1\alpha)$. Figures 4 and 5 illustrate the physical reason for the zero bottom flow condition over the entire domain produced by these boundary conditions. The zero bottom flow in boundary triangles leads to zero bottom flow along characteristics (as long as they are defined) and thus over the entire domain.

The three techniques used to estimate the density-driven partition of the flow can now be compared and evaluated in terms of our original objectives, i.e., to represent the **baroclinic** component of the **flow**; along with the minimum **barotropic** mode (sea surface elevation) such that the bottom flow can be reconciled with the given density and topographic fields.

All three approaches lead to current patterns in the interior which are essentially indistinguishable. Differences occur in the boundary regions and in the small bottom currents. The method of minimizing **potential energy along characteristics using the** reduced equations leads to the highest overall potential energy of the three techniques. In terms of the obvious development of extraneous boundary currents the characteristic method is intermediate with boundary layers weaker than the Green's function solution, but with considerably stronger boundary layers in the natural boundary condition solutions. The characteristic method gives a relatively strong band of bottom currents along the face of the continental slope.

These currents are **suspect and** most likely are related to the **way the** offshore and cross-shelf segments are joined.

The Green's function technique gives a clear overall minimum potential energy solution. Interior bottom currents are very close to zero and seem to suggest that, away from the boundaries, the minimum set-up case consistent with the model dynamics results in quiescent bottom currents. The Green's function minimization of the entire regime does have the disadvantage that it generates energetic boundary currents which are obviously not realistic.

The natural boundary **condition** solution is **computationally** the simplest, and like the Green's function solution, the interior bottom currents are zero. In addition, this technique leads to essentially no boundary layers and extends the zero bottom flow throughout the entire domain, including boundary regions. With this it is possible to interpret the minimum **barotropic** mode in a somewhat different light. The unforced **baroclinic** response of a complex bathymetric region that has adjusted in such a way as to minimize the potential energy **of the sea surface elevation will approach a zero bottom current condition.** The natural boundary condition formulation best yields this "minimum **barotropic**" mode by a circulation that in fact creates a minimum (zero) bathymetric interaction. This differs from the absolute minimum potential energy flow only in the important open cross-shelf boundary regions, and here the natural boundary condition formulation leads to more realistic flow, free from what are known to be extraneous currents.

It is an interesting side note that, given an unforced **geostrophic** plus Ekman flow regime for any region, the only possible steady state circulation will be the case where the **barotropic** and **baroclinic** modes

combine in such a way as to yield a zero bathymetric interaction, which in essence turns off the frictional dissipation.

In Figures 17 and 18 we can see the GS region's response to indirect wind forcing. **This includes the large-scale regional set-up of the sea surface but not local surface Ekman currents.** An examination of these results reveal a number of interesting features and regional characteristics.

The use of the FEM natural boundary conditions allows for a smooth continuation of the solution through boundary regions, so that specifying **surface** elevations anywhere in the model results in a regional circulation pattern with what appears to be transparent boundaries. For example, in 17a and 18a a uniform surface slope is specified across the shelf on the eastern boundary and natural boundary conditions are used along the western boundary. Figures 17b and 18b show the flow that results when the cross-shelf elevations are determined across the middle of the model and both east and west boundaries are determined as the natural boundary conditions. Figures 17c and 18c show the corresponding case forced from the western boundary. It is interesting to note the differences between these cases. There is obviously a length scale associated with the region influenced by any of these cases. To understand these **variations we** may once again consider the Green's function components, which in turn represent just the regional dynamic response of the model. Along the shelf break where bathymetric controls are dominant the parabolic nature of the equations is evident, and extends across the entire model closely following f/d contours. In contrast, the shelf in the nearshore region is nearly flat and bottom friction, the elliptic nature of the equation dominant, and the diffusive character of the solutions are clearly seen. This diffusive scale is of special interest and can be estimated by a scale analysis

of the differential equation. The relevant term in the governing equation is

$$N_2 \nabla^2 \xi$$

Since in non-dimensional form ξ has been scaled to 0 (unity) this term will **only be significant when**

$$\frac{N_2}{L_2} \approx 0 \text{ (unity)}$$

This **defines** a length over which ξ variations must occur if the elliptic term is to be significant, i.e.,

$$L \propto (N_2)^{1/2}$$

This is the appropriate scale length for the Green's function response in relatively flat regions where elliptic nature of the differential equation dominates, **i.e.,**

$$|N_2 \nabla^2 \xi| > |J(\xi, d)|$$

It is also clear from these scaling considerations that the diffusive length scale $(N_2)^{1/2}$ determines the minimum size bathymetric feature that will be effective in the conservation of potential vorticity-dominated, parabolic model response. That is, in the presence of bathymetric variations the flow will follow f/d contours only **down to a scale** length where the diffusive processes become significant, at which point smoothing of the elevation contours will occur. Covering the entire cross shelf region, the solutions show a smooth gradation from one set of dynamic balances to the other. The same characteristics and length **scales** that are seen in the Green's function appear in our hinge solution.

As a final point, the three hinge modes are linearly independent and can be thought of as hinge influence functions. Then, assuming that we have sea surface elevation information at various points along the coast, these can be combined in a logical way. For each point along the coastal boundary (segment a - Fig. 1), a bathystrophic hinge response is calculated. A distribution of sea surface elevation along the coast will be associated with this hinge located at point n along the coast, i.e.,

$$E_n = f_n(s)$$

where $f(s)$ is just the value of the hinge response as a function of the distance s along the coast. Then given m locations along the coastline where the hinge amplitudes h_m are given, the following m equations can be developed:

$$h_m = \int_n c_n f_n(s_m)$$

Form = n a solution is obviously possible, the appropriate weighting amplitudes for all the hinges are obtained in terms of the coefficients (c_n 's). If an infinite number of m locations are chosen, the above equation and formulation clearly degenerate to a continuum and once again give a formal Green's function solution to the model dynamics subject to a linear sea surface slope forcing (hinge mode) across the shelf.

For any particular shelf region or transect, the surface elevation will be the sum of a number of hinge modes; thus, it will not necessarily appear as a uniform cross-shelf profile. Instead it will reflect the appropriate dynamic distribution of the immediate location, plus the weighted contribution from neighboring locations. In a somewhat related study,

Csandady (1978) considered similar dynamics and the regional influence of **local** wind forcing and offshore circulation. His work was for a uniformly sloping wedge-shaped coastal **region** where the parabolic nature of the dynamics was uniformly dominant.

For the present study the three hinge modes shown in Figures 17 and 18 can be considered as an initial numerical approximation to the continuum Green's function. For these the influence function f_n falls off to essentially zero at adjacent hinge points and the weighting factors are locally determined, i.e.,

$$h_m = C_m$$

This means that each hinge **coefficient** will be set at the locally determined (**bathystrophically** balanced) value and the total solution will be the sum of the three hinge modes.

Having examined all of the various modes for the Gondwannal and Shelf region and considered the dynamics of the decomposition from a number of points of view, it is informative to look at the composite flow. We will combine the output of the density-driven and wind set-up responses. Figure 20 shows the results of the natural boundary condition solution for the density-driven response plus the sum **of the hinge** modes representing the coastal set-up case. Figure 21 shows the natural boundary condition solution for the density-driven response minus the sum of the hinge solutions representing a coastal set-down case. Assuming a simple hinge response for the shelf, all possible circulation patterns must be some linear combinations of the modes represented in 12c, 17a, and **17c**.

VII. Conclusions

The linear **diagnostic** model equations have been formally decomposed into a **density-driven response and a wind set-up response**. These responses,

plus an additional non-divergent surface Ekman mode, make up the total flow that can be represented by the model. The density-driven response is made up of **baroclinic** currents driven by the imposed density **field** and by a minimum **barotropic mode** which orients the combined bottom currents in such a way as to satisfy **the** model's dynamic and kinematic constraints.

The model is tested on an analytic, but realistic domain (the **Gon-
dwannaland** Shelf) which includes topographic features representing a broad shelf and continental slope with a shallower bank and large submarine canyon.

Three alternate approaches are used to obtain estimates of the **minimum barotropic** mode. The first, based on characteristic of the reduced model equations, is of historical interest in that it has been used in previous studies. The second solution technique obtains a minimizing potential energy for the sea surface, and thus shows the most relaxed overall regional state that is consistent with the **bathymetry** and density fields. The third method, which depends on the finite element technique, is **computationally** the simplest, and from a theoretical point of view should reduce the **occurrence** of extraneous open boundary currents.

All three of these techniques yield essentially identical interior flows. The finite element method using natural boundary conditions **is** seen to offer the best approximation to the minimum **barotropic** mode, in that it extends the formal minimum potential energy solution **smoothly** throughout the cross-shelf boundary regions. From a physical point of view, the **minimum barotropic** mode represents a "minimum bathymetric interaction" i.e., **barotropic** and **baroclinic** modes that give zero bottom **flow**. Conceptually this is a natural extension of the offshore level of no motion introduced by the dynamic heights method. In addition it can be seen **that**, given unforced **barotropic, baroclinic** and bottom Ekman modes, this is

the only possible steady **invisid** circulation pattern. Within **the** context of the linear model formulation, the density-driven response contains all of the independent circulation information available from the density data. The development of the density-driven response can be carried out once for each set of STD or CTD data available for the study region, but beyond that no other independent density related circulation modes are possible.

The wind set-up response of the model can be represented by a number of hinge, or cross-shelf profile modes. the known profile can be applied anywhere within the model when the finite element method with natural boundary conditions is **used**. The region of influence of any single **cross-shelf** profile depends upon the topography and can be explained in terms of the joint elliptic and parabolic nature of the governing partial differential equation. This dependence can also be clearly demonstrated by the component Green's function responses that were developed. These domains of influence for the hinge or cross-shelf profile modes define the need for boundary input data and the spatial scale that must be resolved by observations.

Having developed the response characteristics of the model region, it is obvious that **these** patterns could be usefully employed to design the minimum resolution observational grid needed to study the area, For a **linear** system, the other relevant scale would be the **length** associated with the forcing (large-scale winds) that set up the cross-shelf profiles.

The total regional circulation for the model domain may now be represented by a simple linear combination of the density response mode and the various hinge or cross-shelf profile modes, plus a non-divergent surface Ekman drift. Since there is only one density response mode for each set

of STD or CTD data, and the wind response modes are all dependent only on the bathymetric characteristics of the region, the procedure of applying the **model** to a study region is greatly simplified. In addition **to increased** model efficiency, these modes are seen to represent fundamental physical processes that can be directly related to empirical data and can be used to obtain measures of success for predicted currents, as well as in the design of observation arrays.

Acknowledgements

The research described in this report has been funded in part by the BLM sponsored Outer Continental Shelf Assessment Program under RU #140. During the course of **the work** Dr. Robert J. **Stewart has offered** many helpful comments and his contribution is gratefully acknowledged.

REFERENCES

- Beardsley, Robert C. and Bradford **Butman** (1974): Circulation on the New England continental shelf; response to strong winter storms, Geophys. Res. Letters **1(4)**; pp 181-184.
- Cole, Julian (1968): Perturbation Methods in Applied Mathematics, **Blaisdell**, New York, 260 pp.
- Courant**, R. and D. **Hilbert** (1962): Methods of Mathematical Physics, Vol. II, **Interscience** Publishers, New York, NY, 830 pp.
- Csanady, **G.T.** (1978): The Arrested Topographic Wave, *JPO* 8(1); pp 47-62.
- Galt, **J.A.** (1975): Development of a simplified diagnostic model for the interpretation of oceanographic data. NOAA Technical Report ERL 339-PMEL 25, National Oceanic and Atmospheric Administration, U.S. Department of Commerce, Washington, DC, 46 pp.
- Galt, **J.A.** (1976): Circulation studies on the Alaskan Continental Shelf off the Copper River Delta. National Oceanic and Atmospheric Administration, U.S. Department of Commerce, Washington, DC, 46 pp.
- Galt, **J.A.** (1977): A diagnostic circulation of the flow in the vicinity of Kodiak, *EOS*, Vol. 58, No. 12, p. 1173 (Abstract only).
- Galt, **J.A.** and **C.H. Pease** (1977): The use of a diagnostic circulation model for oil trajectory analysis, Proceedings of 1977 Oil Spill Conference, March 8-10, New Orleans, Louisiana, pp 447-454.
- Royer, T. (1978): Personal communication, manuscript in preparation.
- Stommel**, H. (1948): The westward intensification of wind-driven ocean currents, American Geophysical Union, Transactions, Vol. 29, No. 2, pp 202-206.

Strang, G. and G.J. Fix (1973): An Analysis of the Finite Element Method, Prentice-Hall Inc., **Englewood** Cliffs, NJ, 306 pp.

Watabayashi, G. and J.A. Galt (1978): A finite element technique for a diagnostic shelf circulation model. NOAA Technical Report (in press).

Wunsch, C. (1977): Determining the general circulation of the oceans: a preliminary discussion, Science, 196, pp 871-875.

Zienkiewicz, O.C. (1971): The Finite Element Method in Engineering Science, McGraw-Hill Publishing Co., New York, NY, 521 pp.

TABLE 1 NONDIMENSIONAL CONSTANTS USED IN THE GONDWANALAND SHELF

D0=-1.00.

D1=50000

D2=49.

D3=7.00

D4=50.

D5=3.0

D6=1.5

D7=1.0

D8=3.14159/2.

D9=-500.

D10=4.0

D11=80.

D12=-1.0

X0=3.5

X1=1.5

Y1=1.0

Y2=2.0

Y3=5.0

Y0=2.5

$$DSHELF = D0 - D1 / (D2 + \exp(D3 * Y * Y)) + D1 * (Y - Y2) / (Y3 - Y2)$$

$$DBANK = D4 * \exp(-(D5 * (X - X0)**2. + D6 * (Y - Y0)**2.))$$

$$DCANYON = \exp(-D7 * (Y - Y1)**2. - D10 * (X - X1)**2.) * \cos(D8 * (X - X1)) * D9 * (1. - \exp(D12 * Y**4.))$$

RH00=1.032

A=.00025

B=.0005

C=1./200.

$$RHO = RH00 - (A * X + B * Y) * \exp(-C * Z)$$

$$ALPHA = RHO * D - (A * X + B * Y) * (1 - \exp(C * (-D))) / C$$

Figure Captions

- Figure 1 General configuration of typical continental shelf study region.
- Figure 2 Example of density field with cross isobath flow for use in an analytic example of **model** solutions.
- Figure 3 Surface elevation contours for secondary **barotropic** flow generated in response to cross isobath **baroclinic** forcing.
- Figure 4 Diagram of **arbitrary** triangle showing the relationship between the independent variables depth and density; their associated gradients ∇d and $\nabla \alpha$, and the **geostrophic** components of the bottom current.
- Figure 5 Series of triangles connected by an isobath, or characteristic for the reduced equation.
- Figure 6 Triangle intersected by an isobath with surface elevations determined at the ends of the transect.
- Figure 7 Demonstration of interpolation technique used to obtain boundary values for the case where f/d characteristics do not intersect the model except at one point.
- Figure 8 Demonstration of interpolation technique used to obtain boundary values for the case where f/d characteristic extends along the edge of the model for two or more boundary points.
- Figure 9 Grid system used for density driven response study on the **GS** region representing a square domain of 5 x 5 non-dimensional units.
- Figure 10 Bathymetric chart of the Gondwanaland shelf **model** domain showing the shelf section with a shoal to the east and a large submarine canyon to the west.
- Figure 11 Alpha field (bottom pressure) deviations along the bottom of the model domain.
- Figure 12 **Contours** of surface **elevation indicating surface stream lines** for the minimum **barotropic** mode. a) method of minimizing potential energy along the characteristics of the reduced equation. b) Green's function minimization of total potential energy. c) Finite element method of natural boundary conditions.
- Figure 13 Green's function components representing model response. a) non-homogeneous forced mode reflecting the density distribution and offshore dynamic heights. b) homogeneous **model** response to a uniform displacement of the offshore region relative to the shelf region. c) homogeneous response to a unit displacement of one boundary point.

- Figure 14 Surface current vectors for the density driven response with the minimum **barotropic** mode a) method of minimizing potential energy along the characteristics of the reduced equation. b) Green's function minimization of total potential energy. c) Finite **element** method natural boundary conditions.
- Figure 15 Bottom current vectors for the density driven response a) method of minimizing potential energy along the characteristics of the reduced equation. b) Green's function minimization of total potential energy. c) Finite element method natural boundary conditions.
- Figure 16 Triangular mesh used for the wind set-up partition of the GS region study.
- Figure 17 Surface elevation contours for the hinge response modes associated with the homogeneous wind set-up partition of the **model** equations a) eastern boundary set as hinge profile, b) central cross shelf transect set as hinge profile, c) western boundary set as hinge profile.
- Figure 18 Current vectors for the hinge response modes associated with the homogeneous wind set-up partition of the model equations. a) eastern boundary set as hinge profile. b) central cross shelf transect set as hinge profile. c) western boundary set as hinge profile.
- Figure 19 **$J(\alpha, d)$ Baroclinic** forcing in density driven response given by the joint **baroclinic**, bathymetric interaction. Shaded area indicates negative values.
- Figure 20 Sum of the density driven response and wind set-up response (hinge modes) for a case representing winds from the east. a) sea surface elevation contours. b) surface current vectors. c) bottom current vectors.
- Figure 21 Sum of density driven response and wind set-up response (hinge modes) for a case representing winds from the west. a) sea surface **elevation contours**. b) **surface current vectors**. c) **bottom current vectors**.

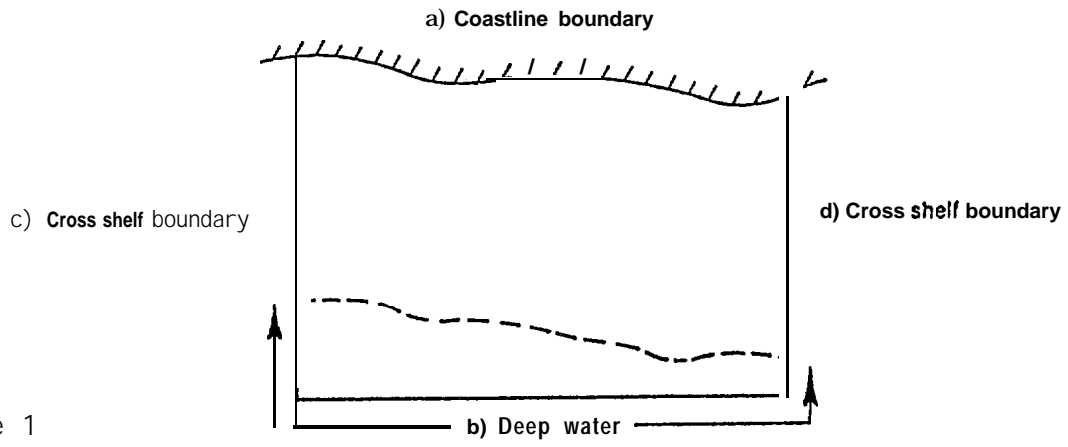


Figure 1

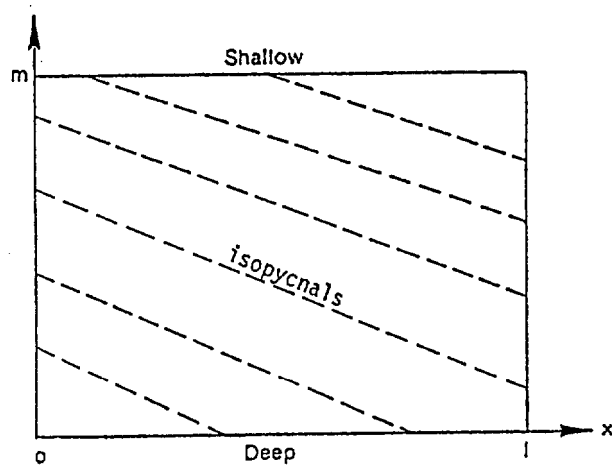


Figure 2

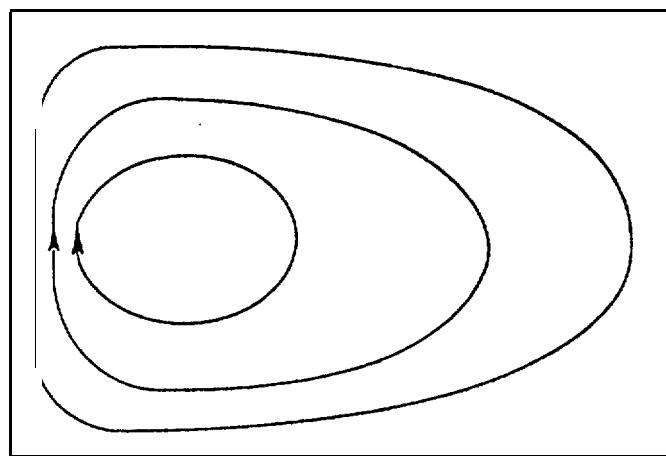


Figure 3

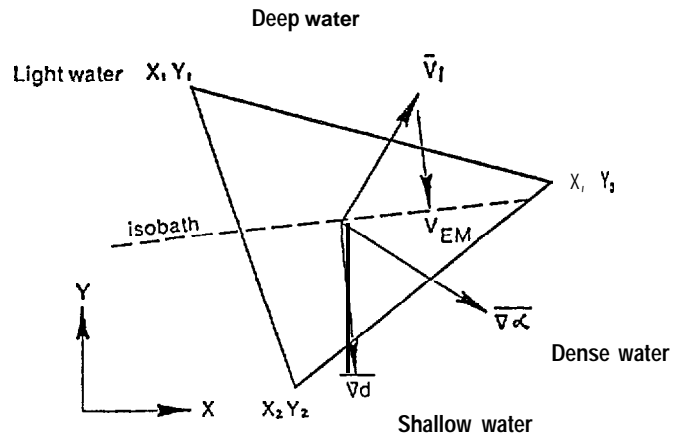


Figure 4

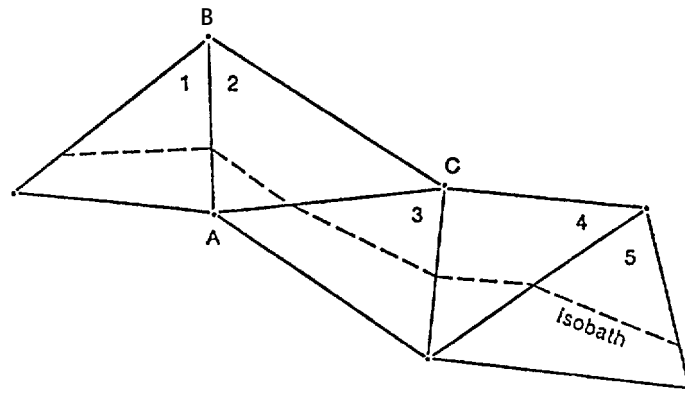


Figure 5

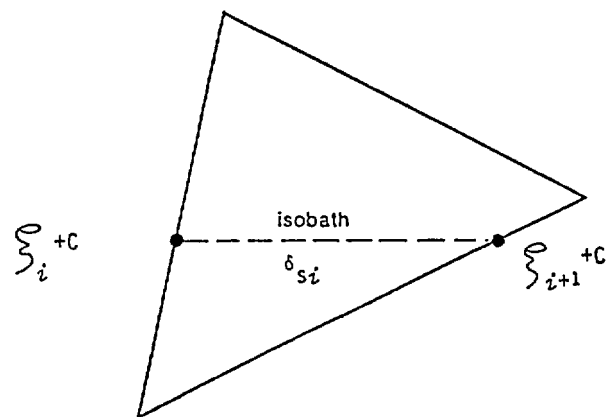


Figure 6

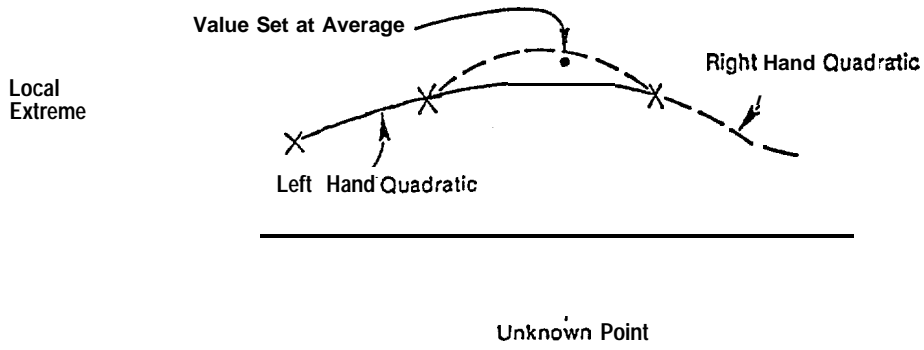


Figure 7

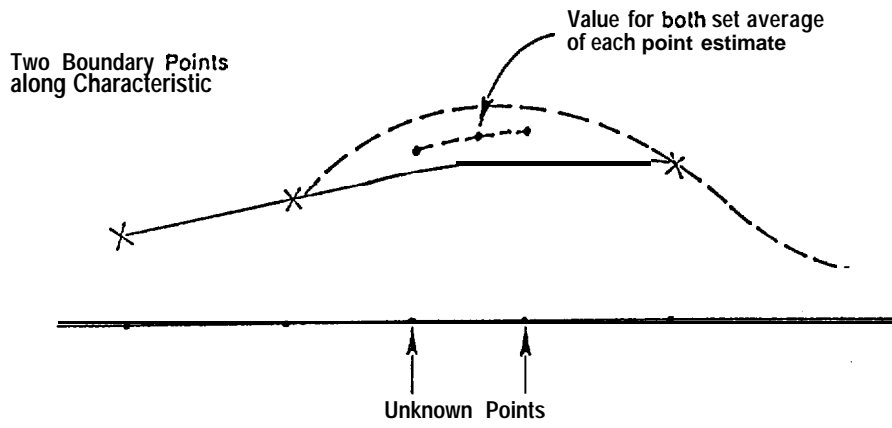


Figure 8

509

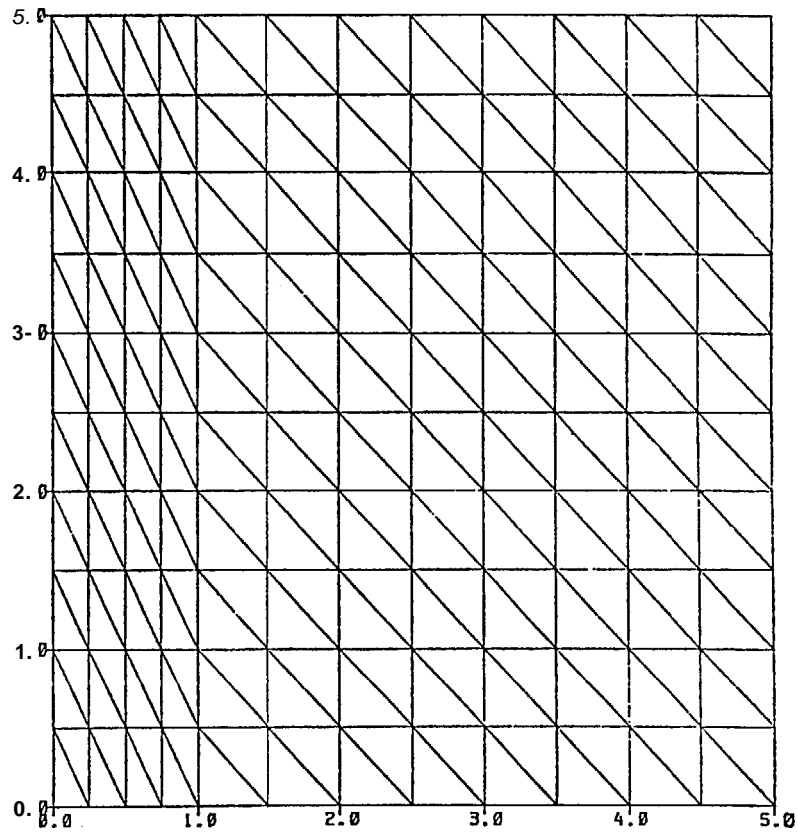


Figure 9

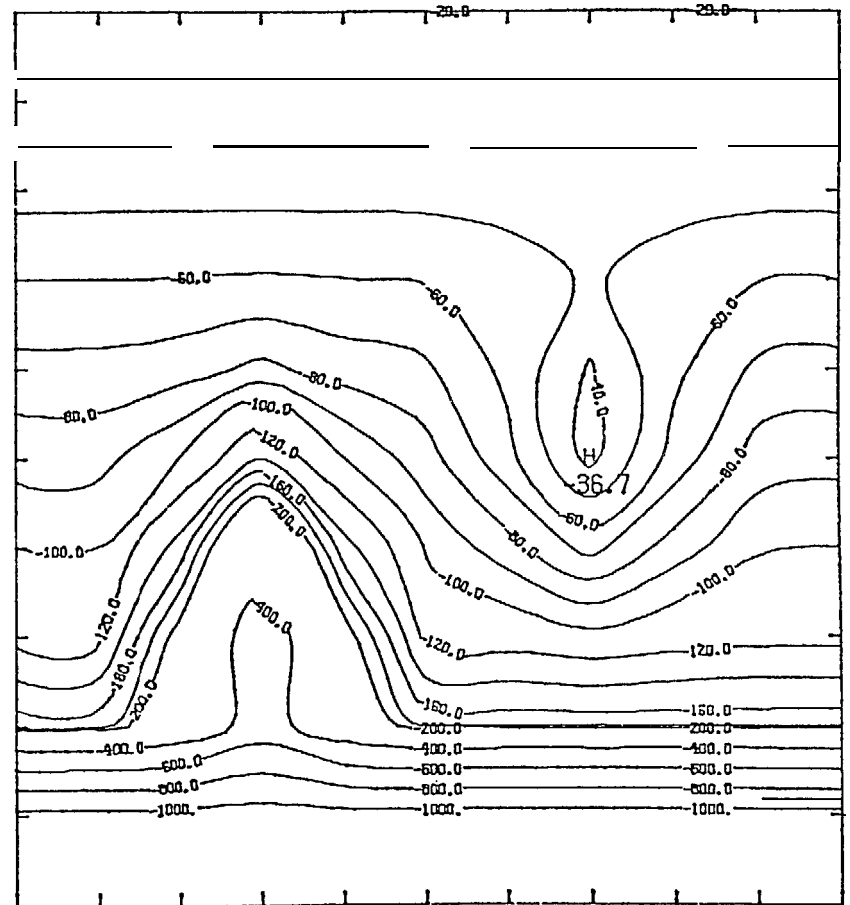


Figure 10

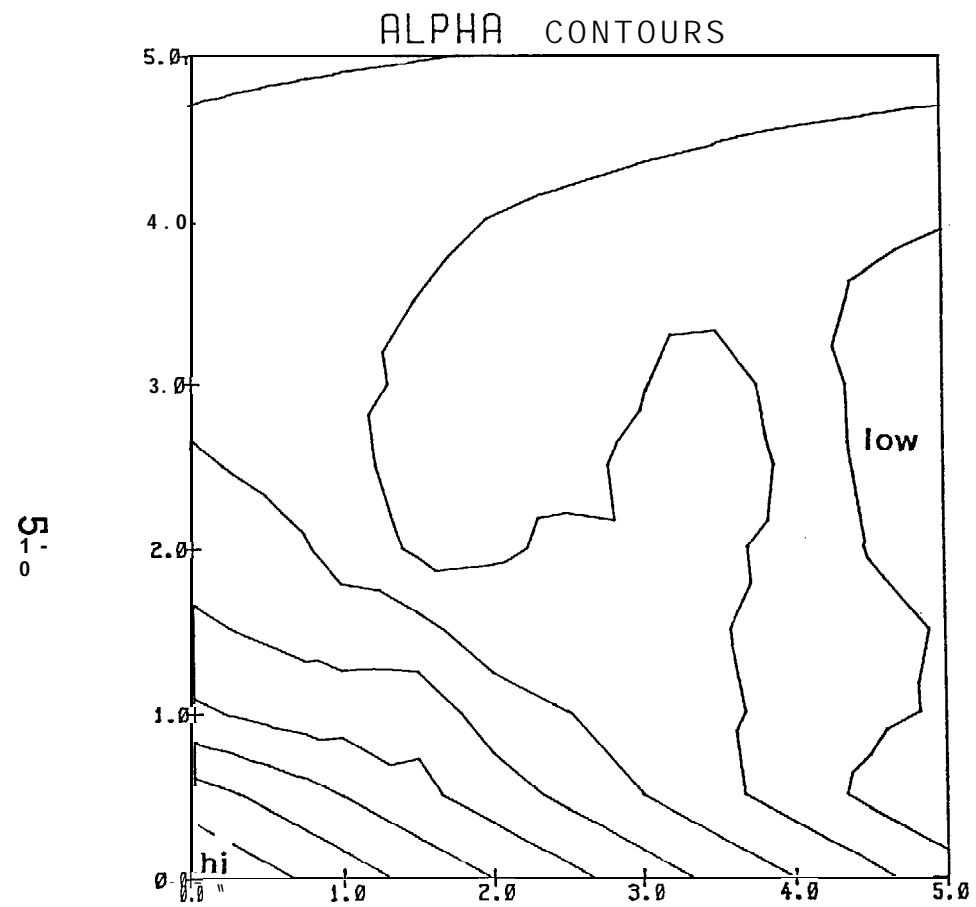


Figure 11

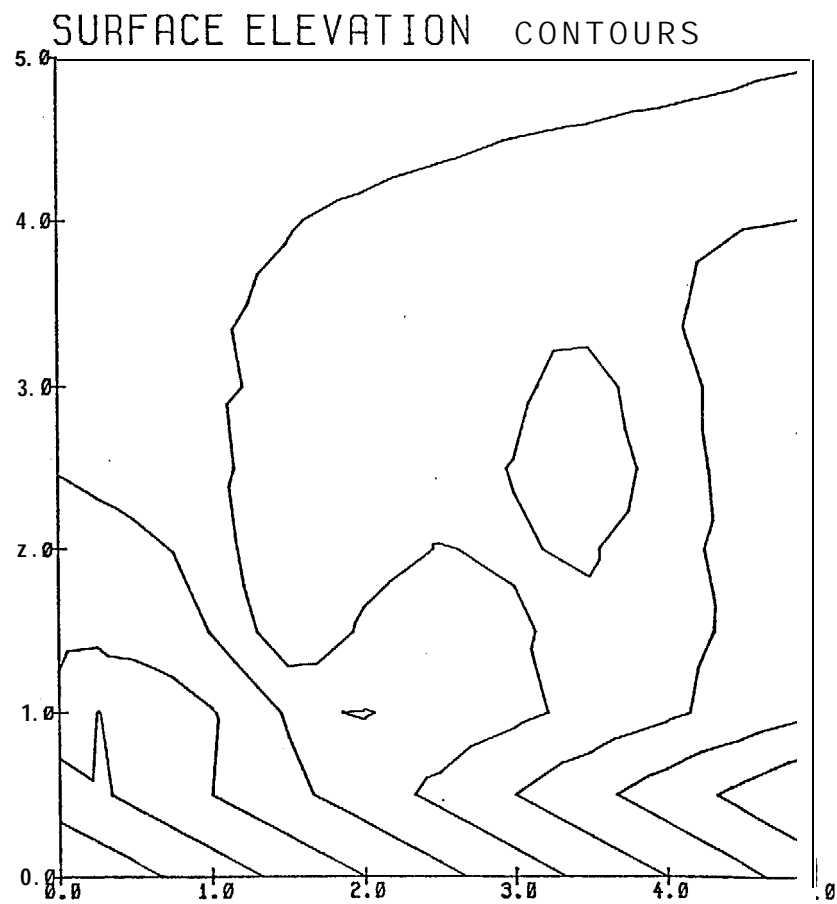


Figure 12a

511

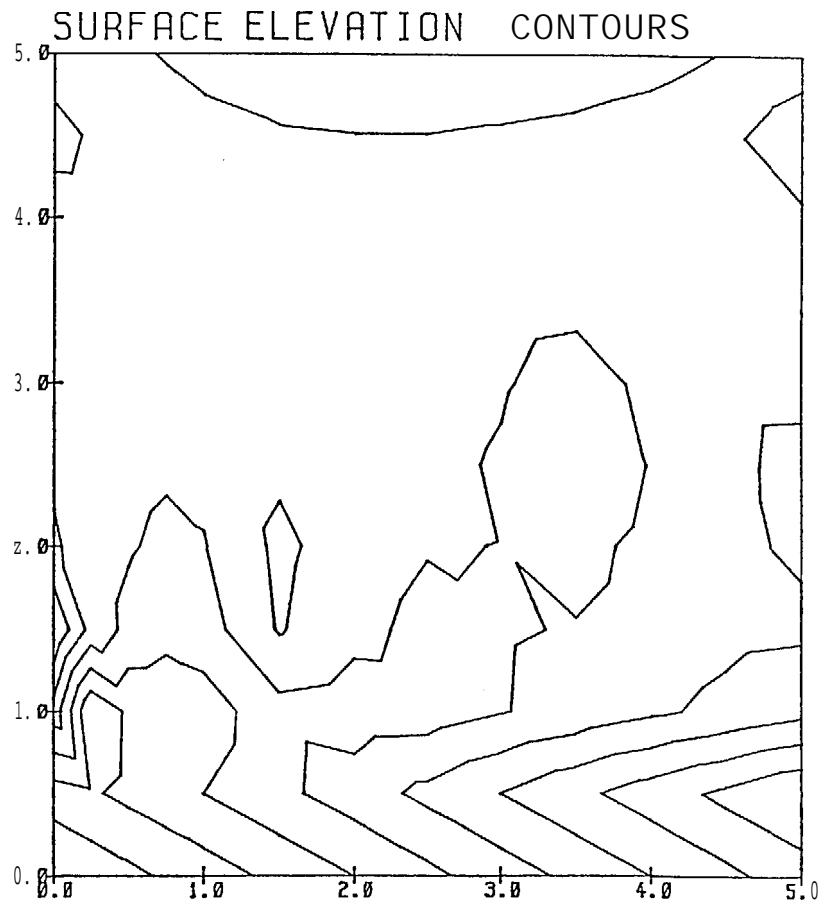


Figure 12b

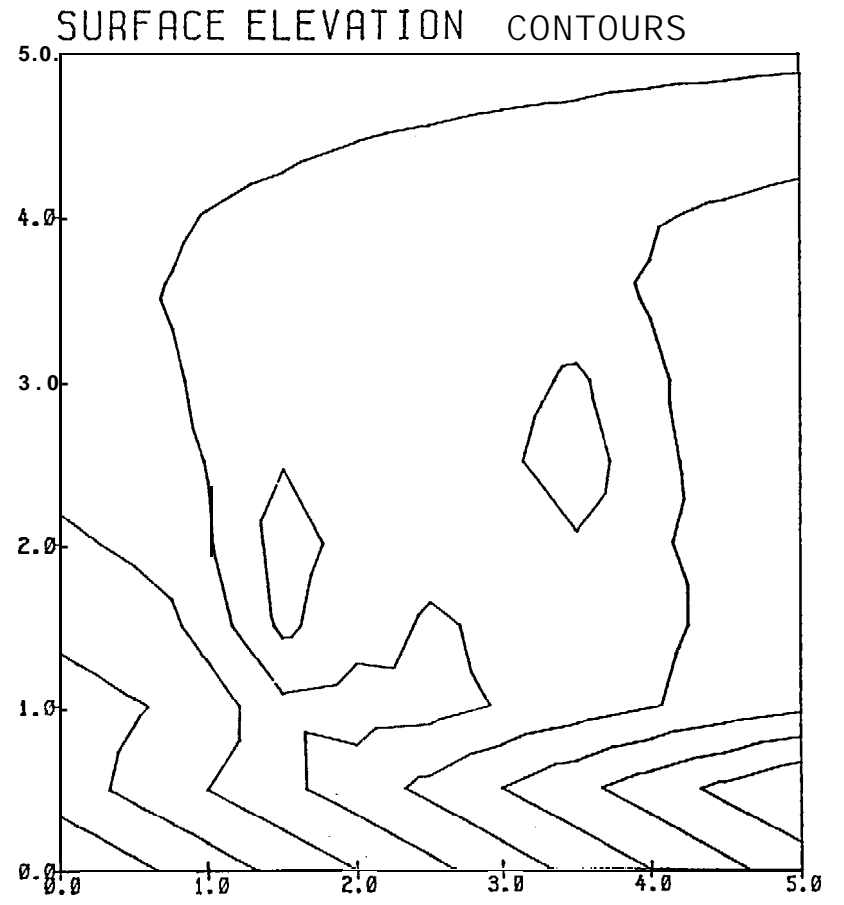


Figure 12c

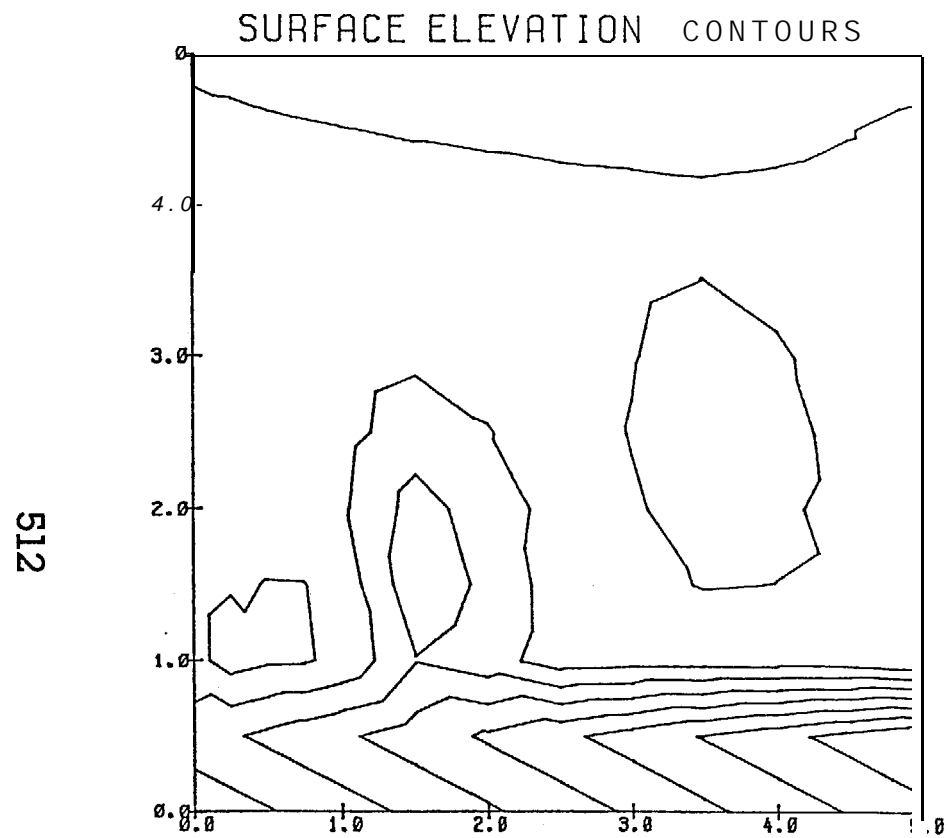


Figure 13a

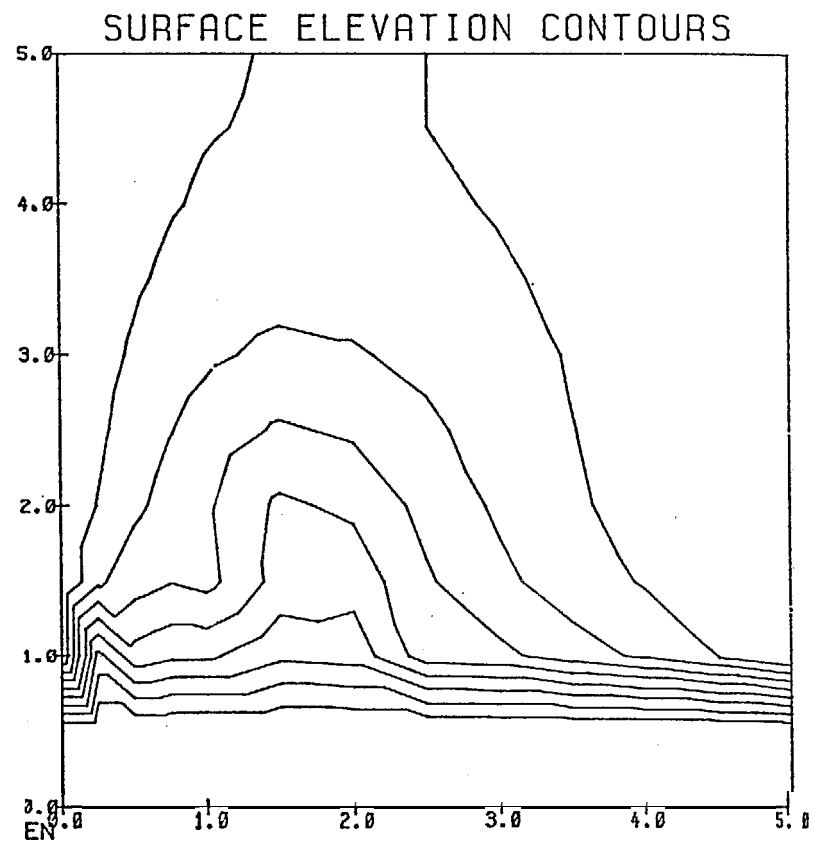
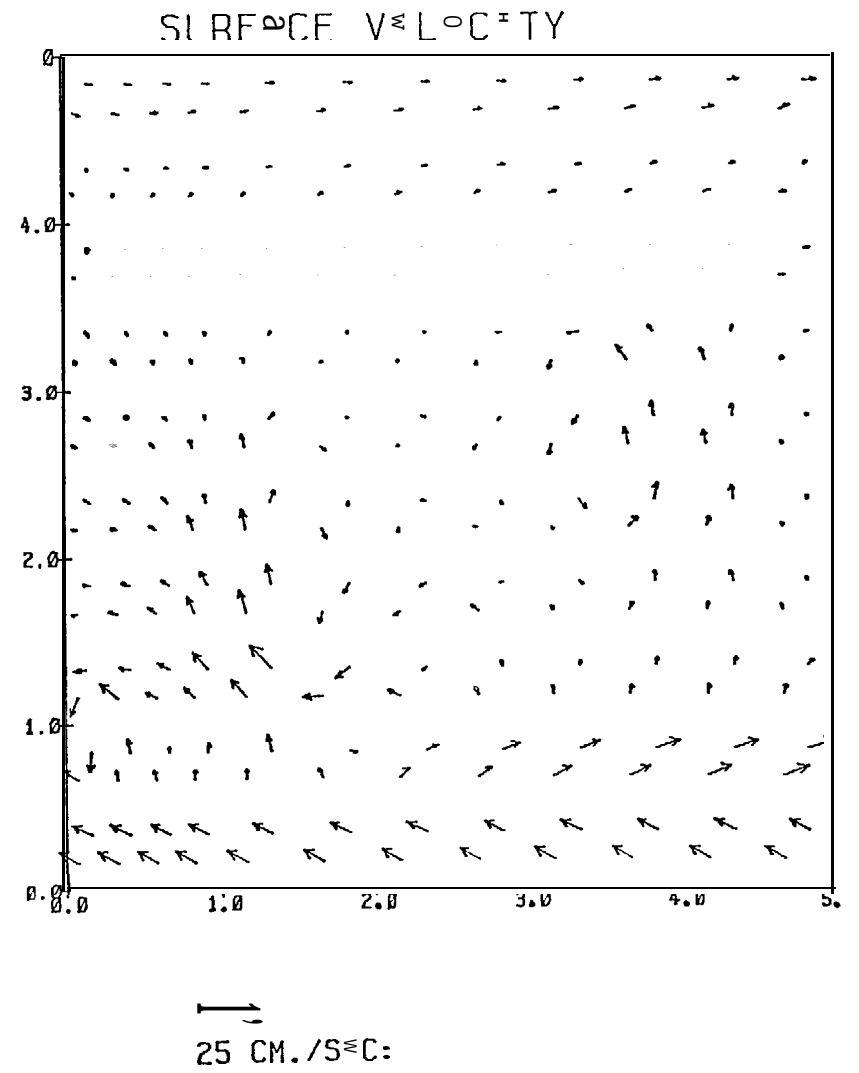
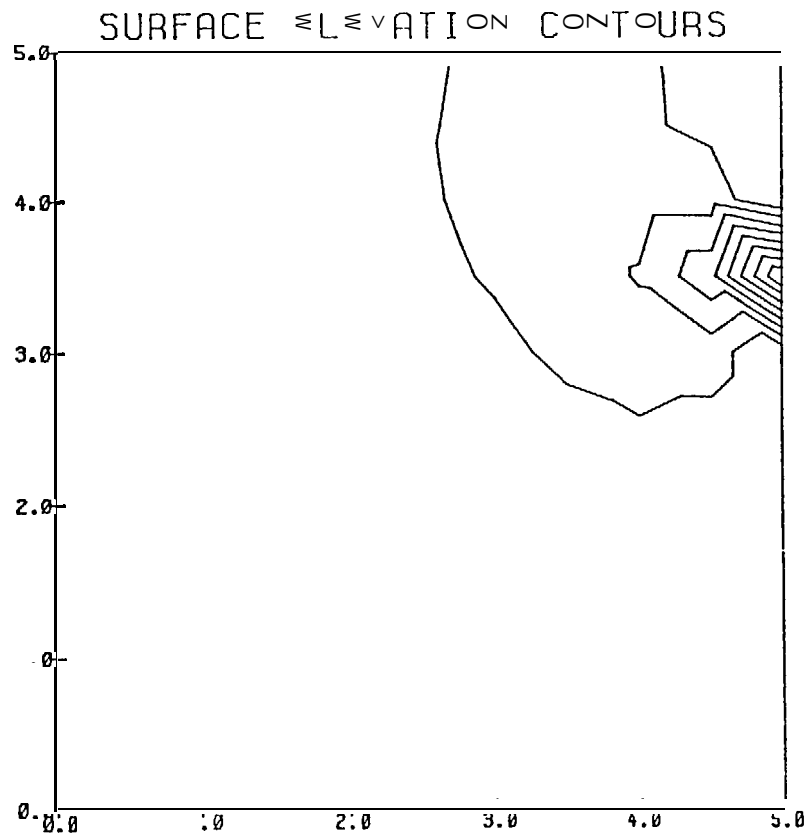
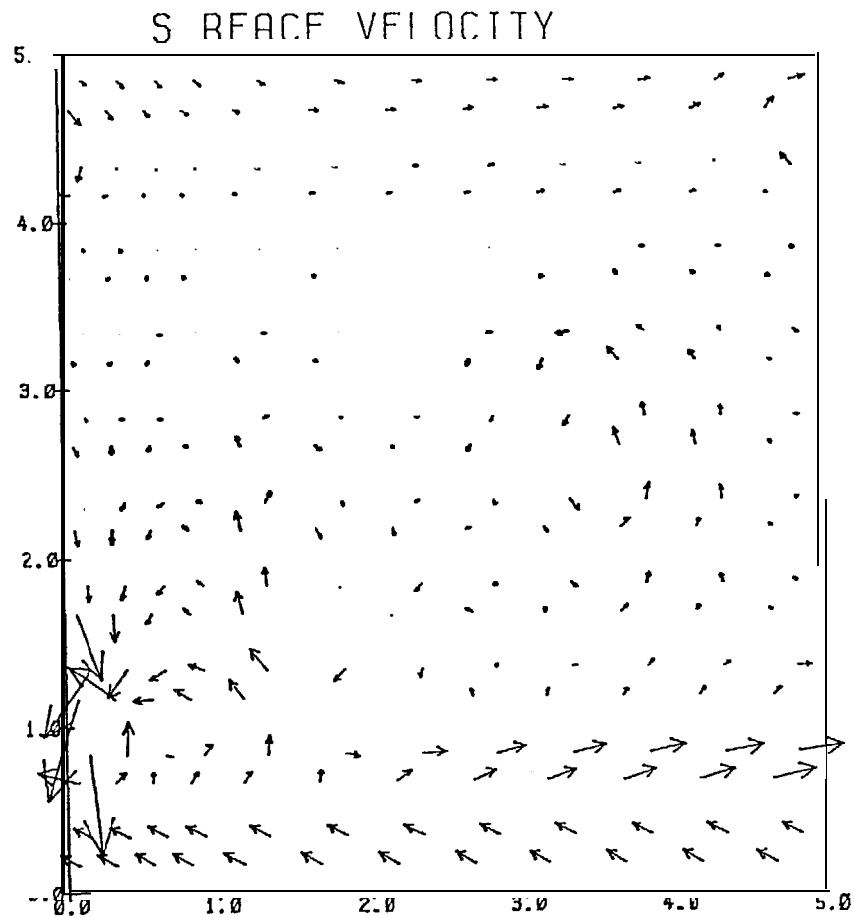


Figure 13b

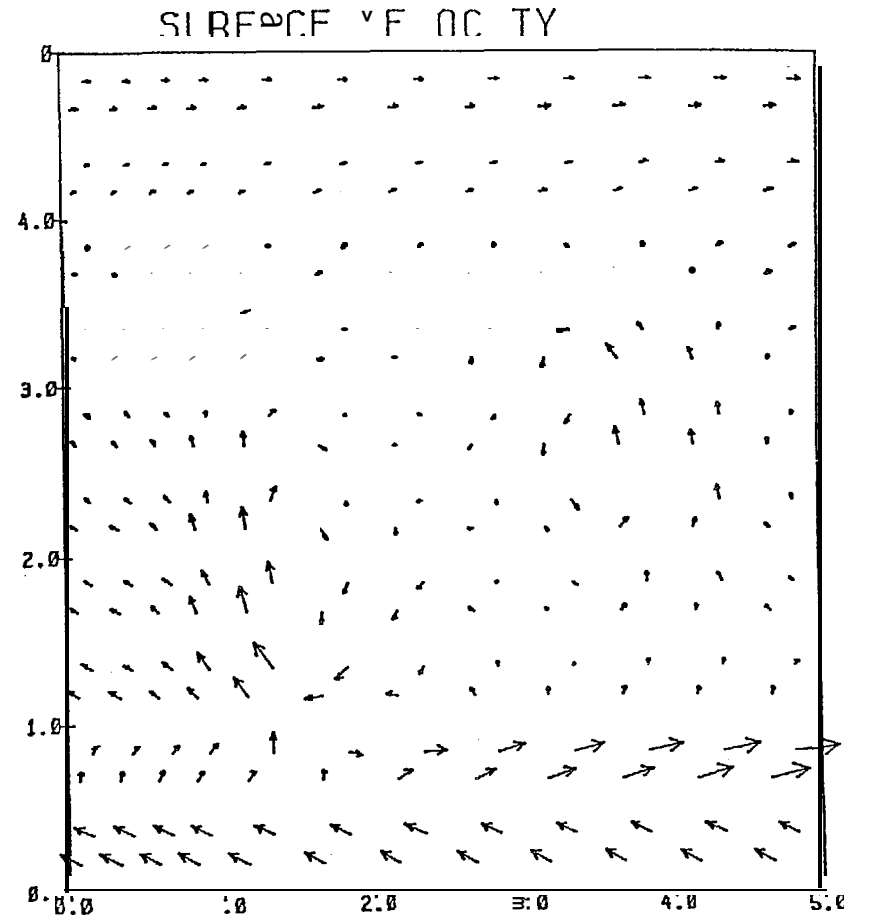


514



→
25 CM./SEC.

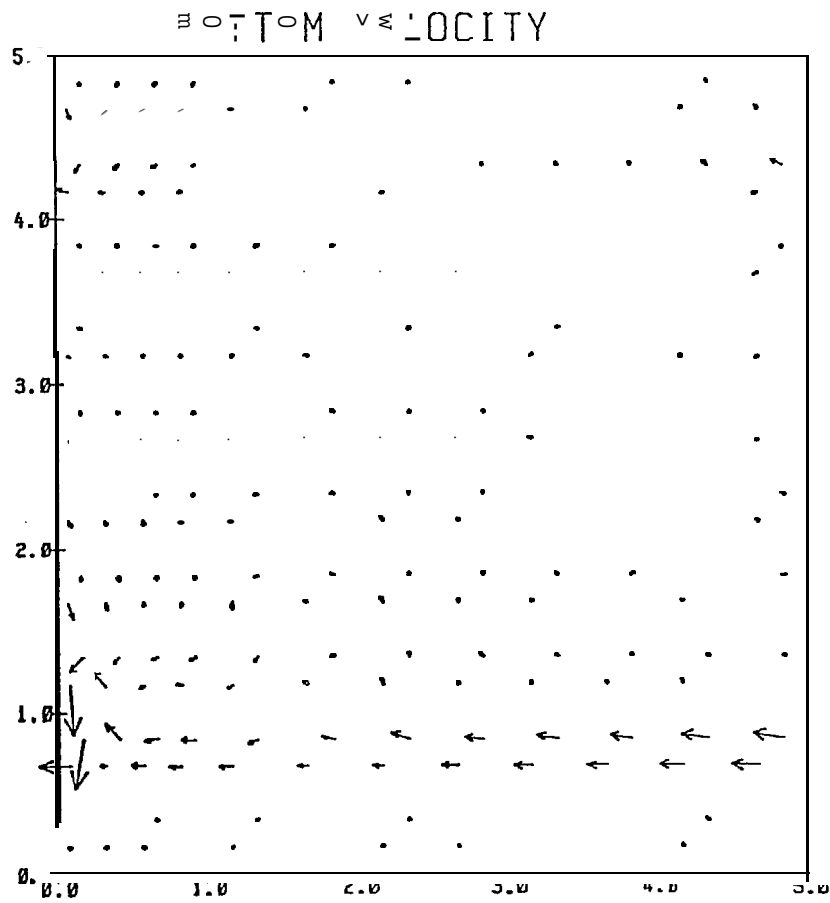
Fi 14b



→
25 CM./SEC.

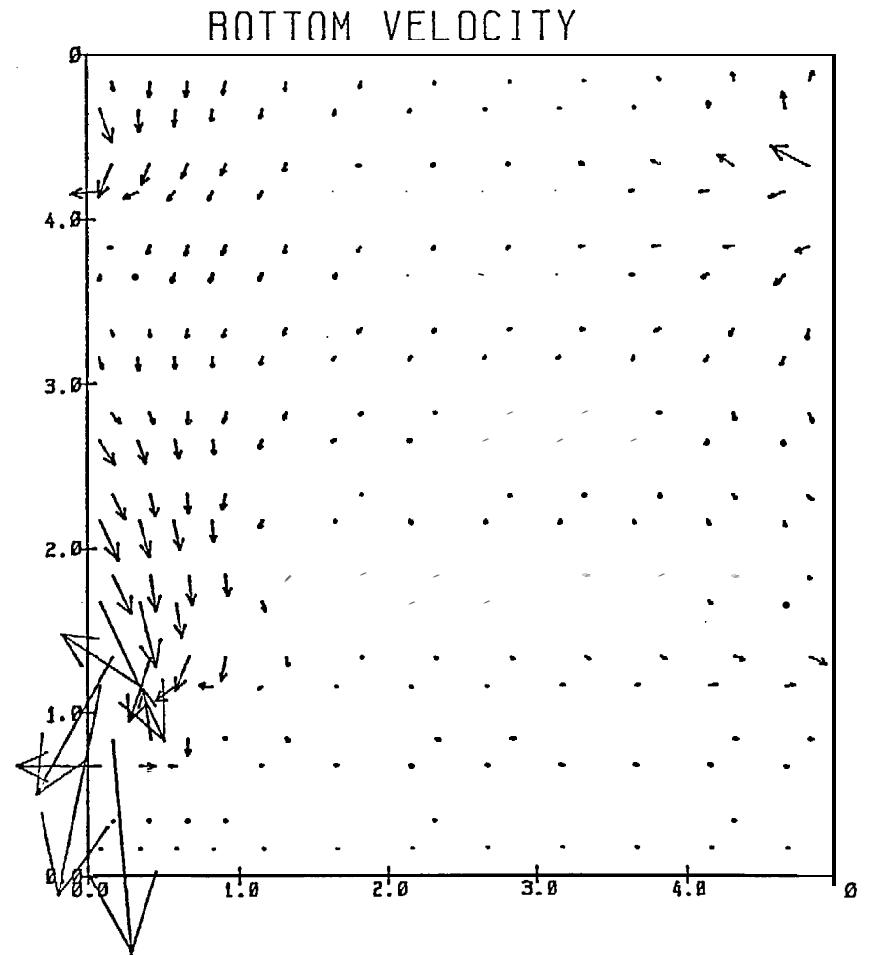
Figure 14c

515



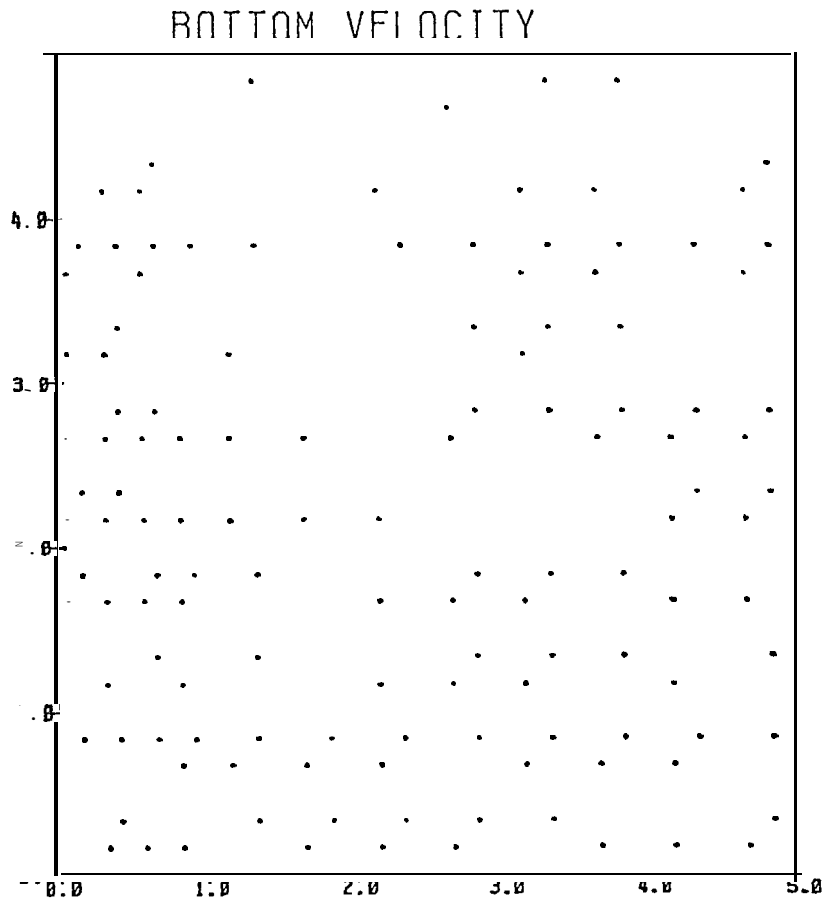
25 CM./SEC.

Figure 15a



25 CM./SEC.

Figure 15b



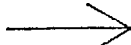

 25 CM./SEC.

Figure 15c

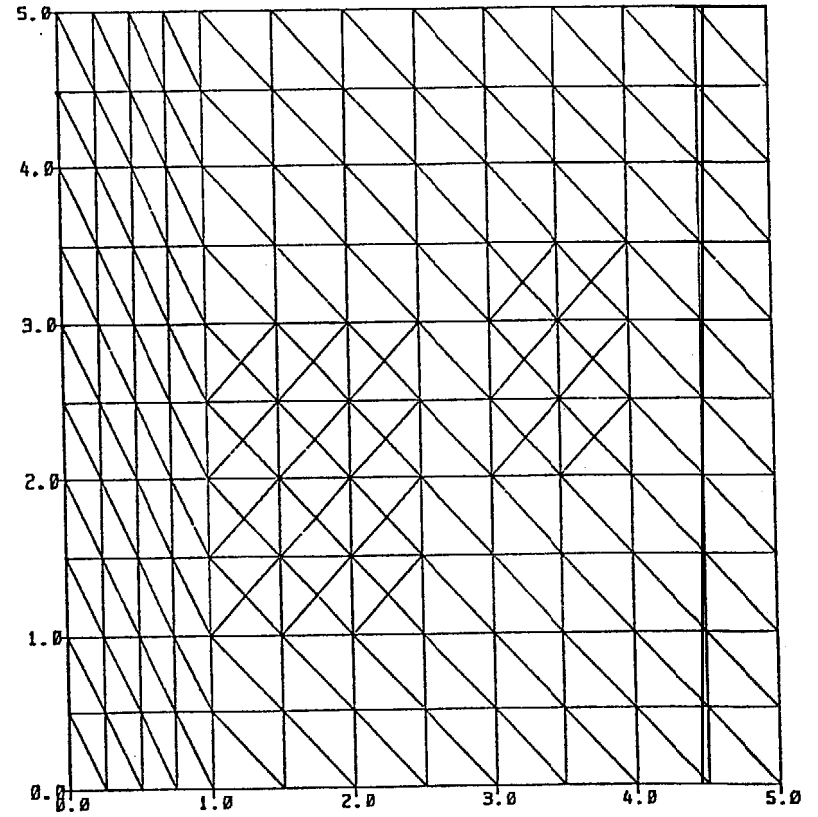


Figure 16

517

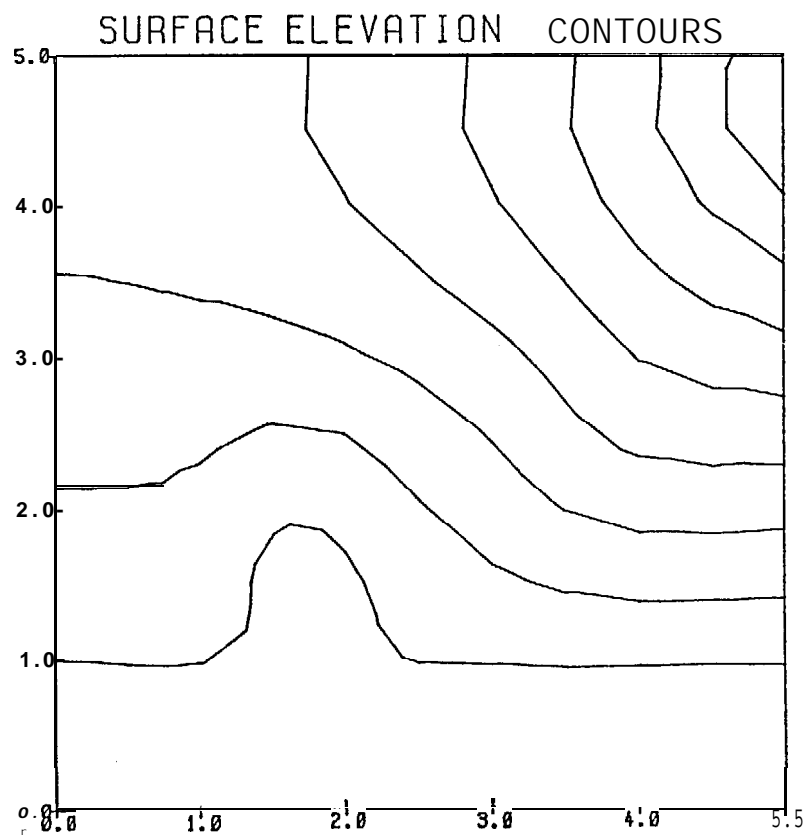


Figure 17a

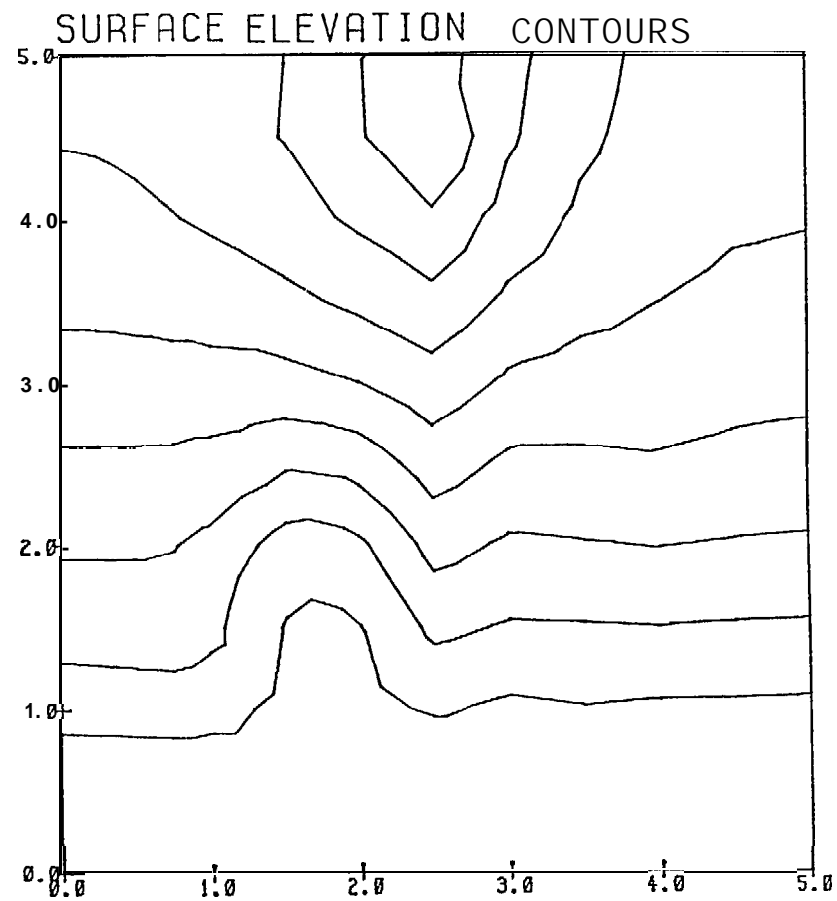


Figure 17b

518

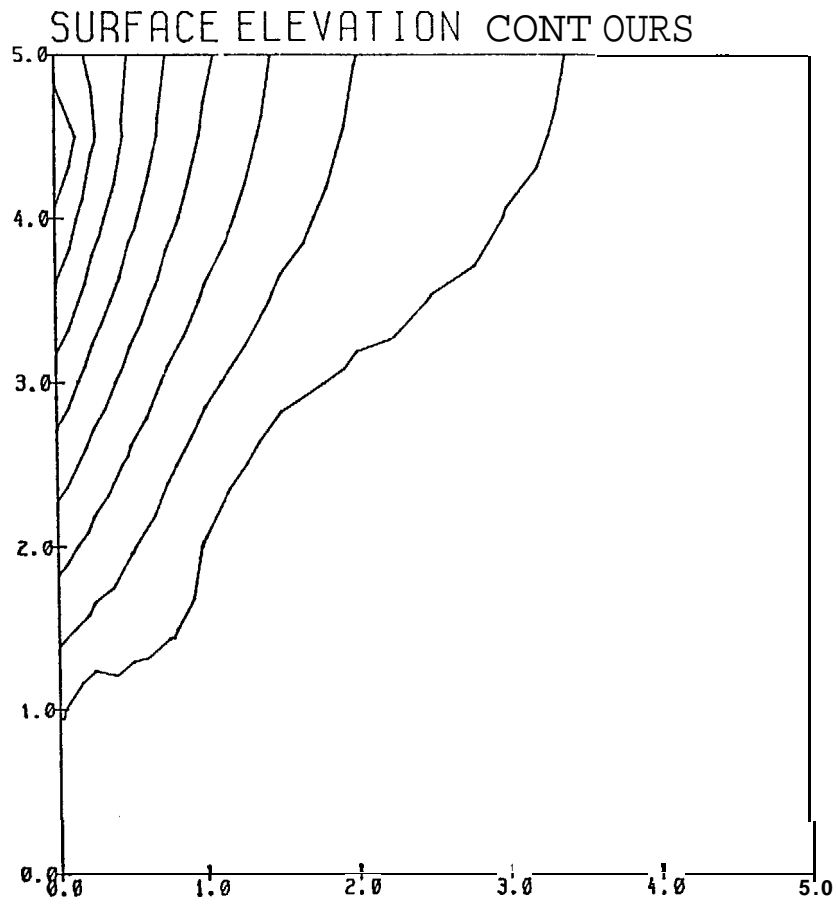
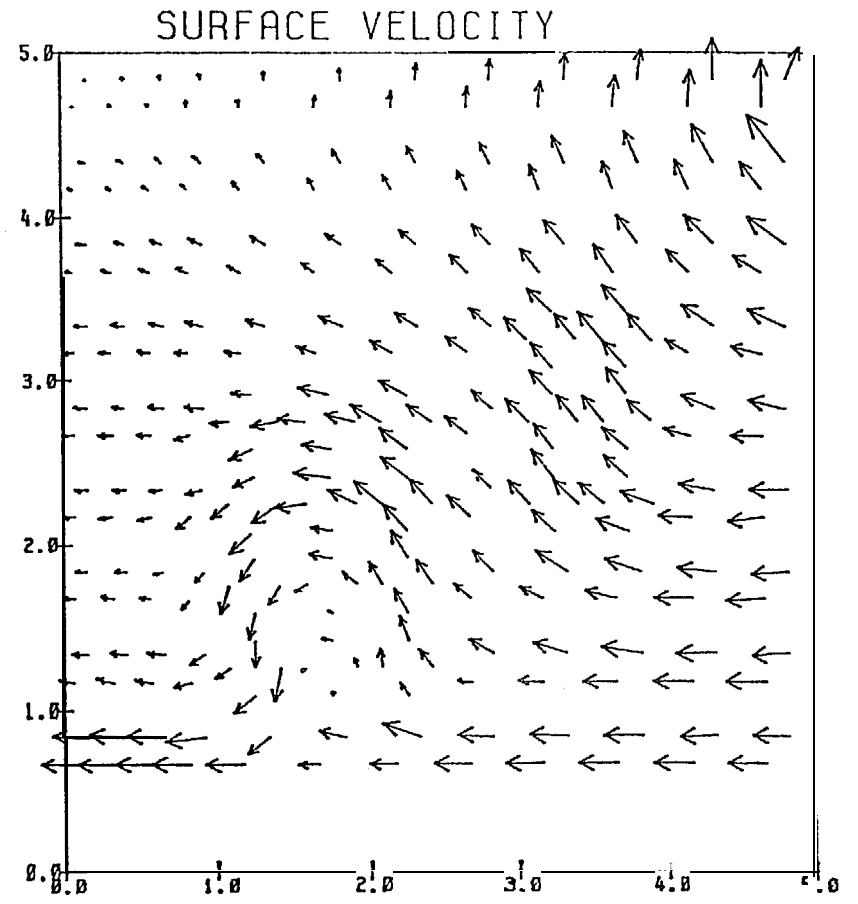


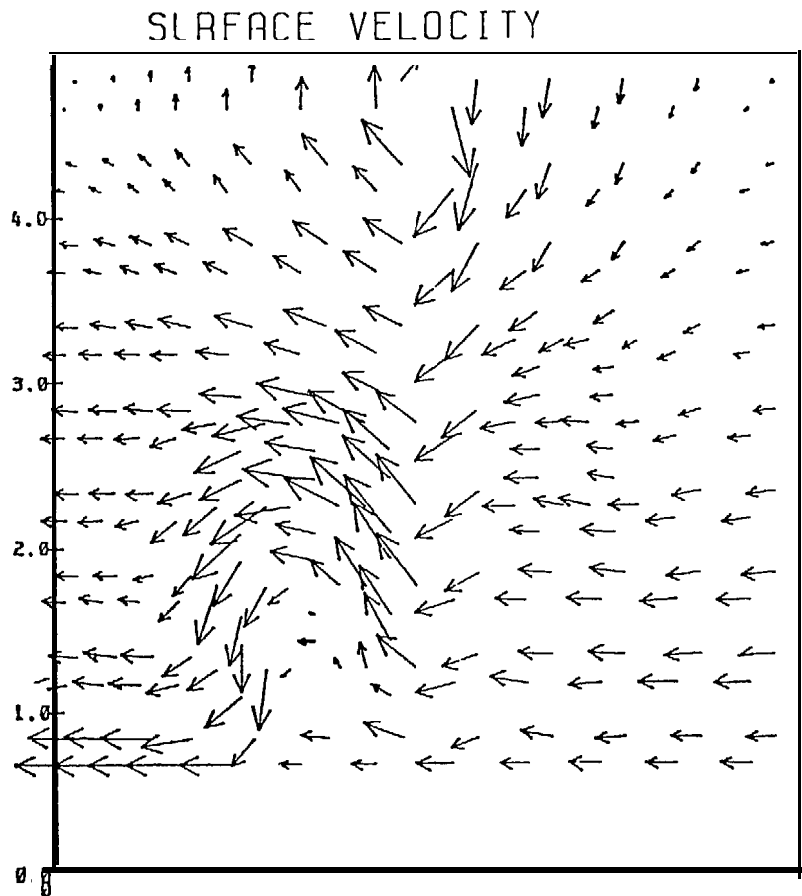
Figure 17c



→
5 CM. / SEC.

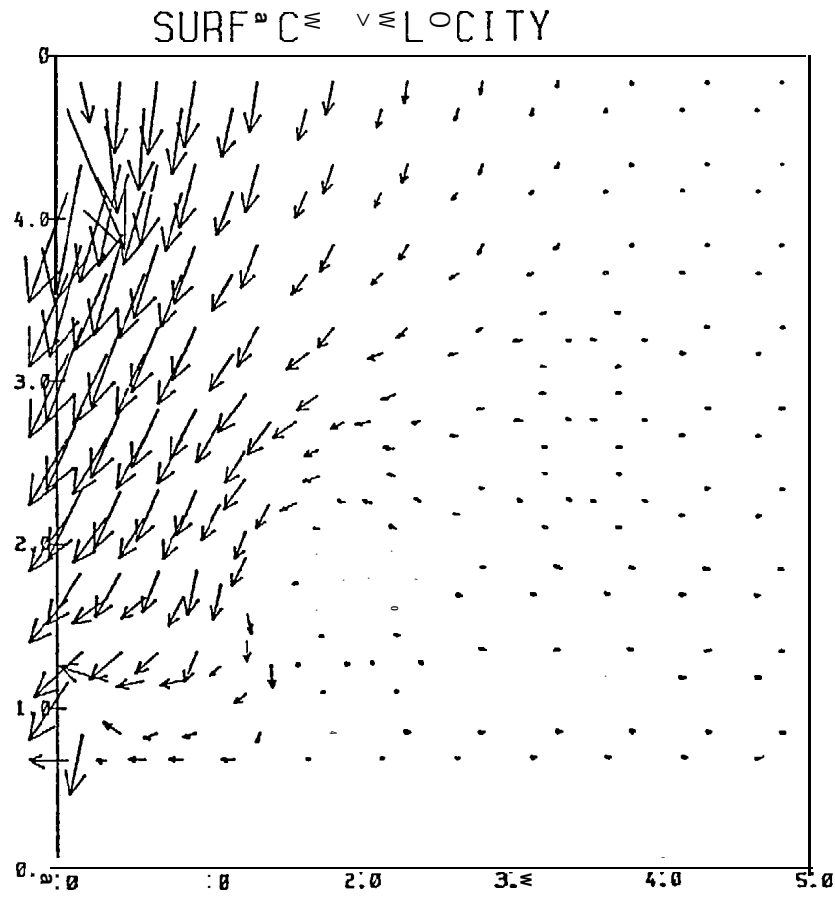
Figure 18a

519



→
5 CM./SEC.:

Figure 8b



→
5 CM./SEC.

Figure 18c

520

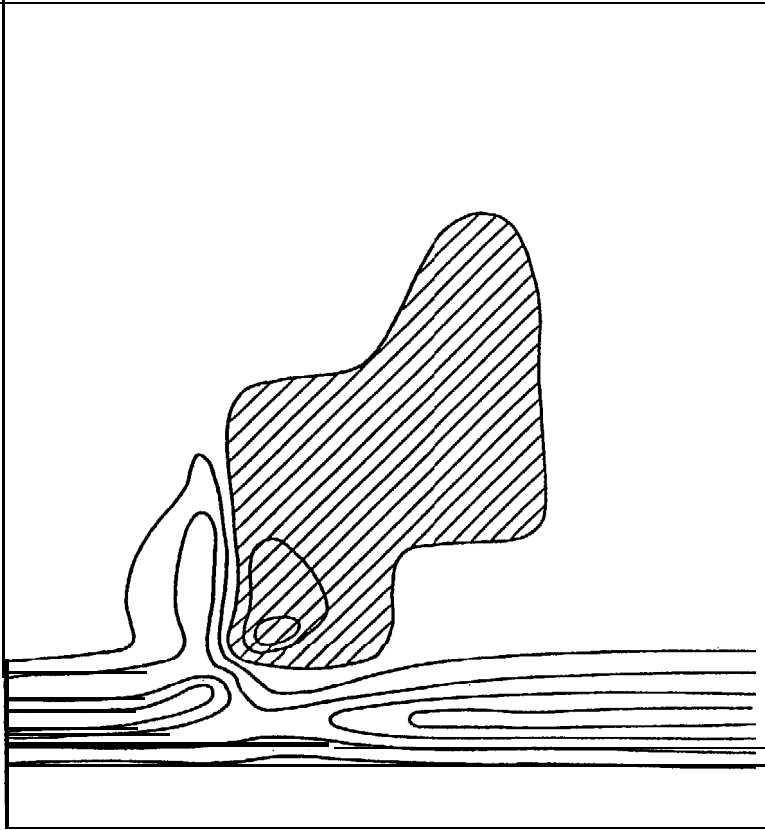


Figure 19

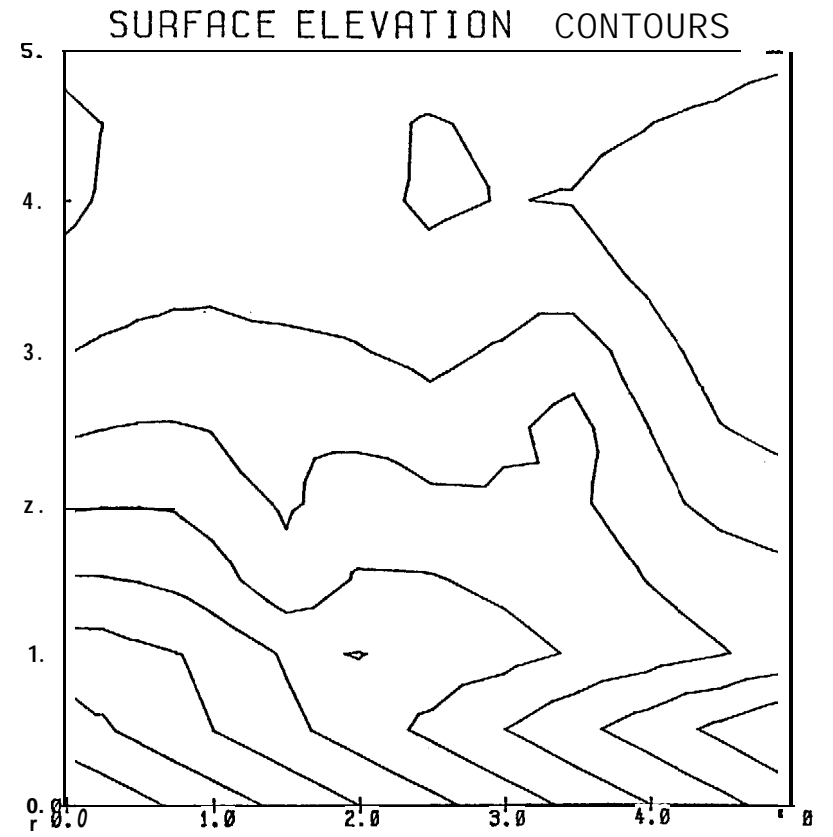
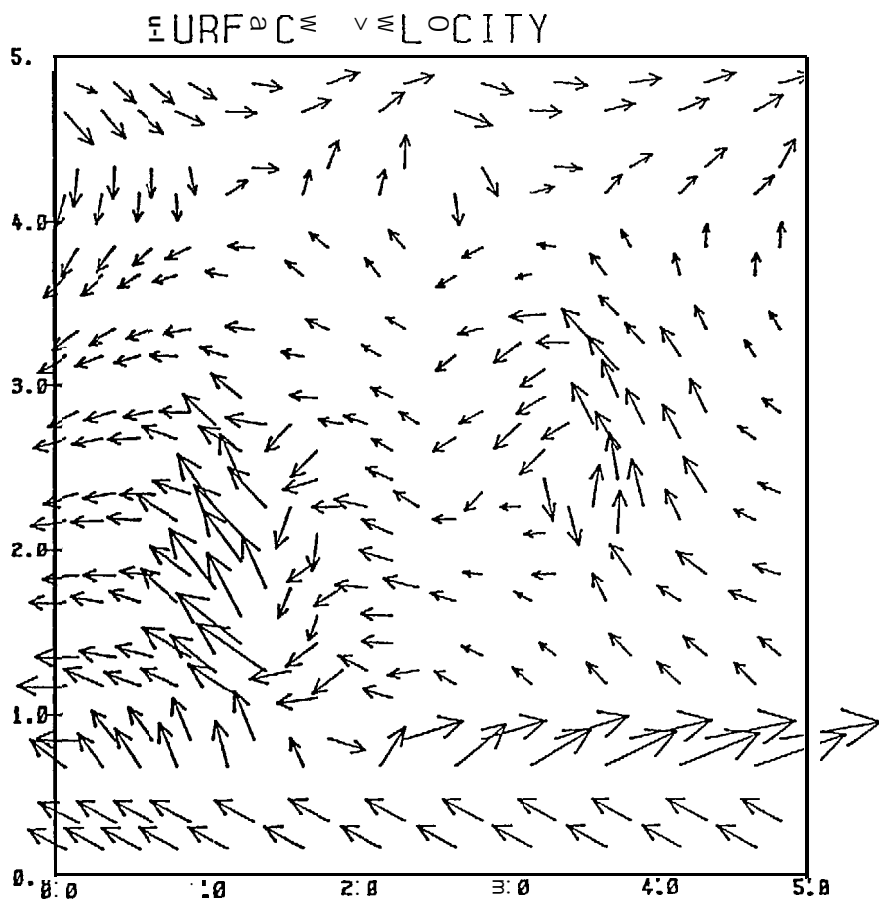


Figure 20a

521



→
25 CM./SEC.

Figure 20b

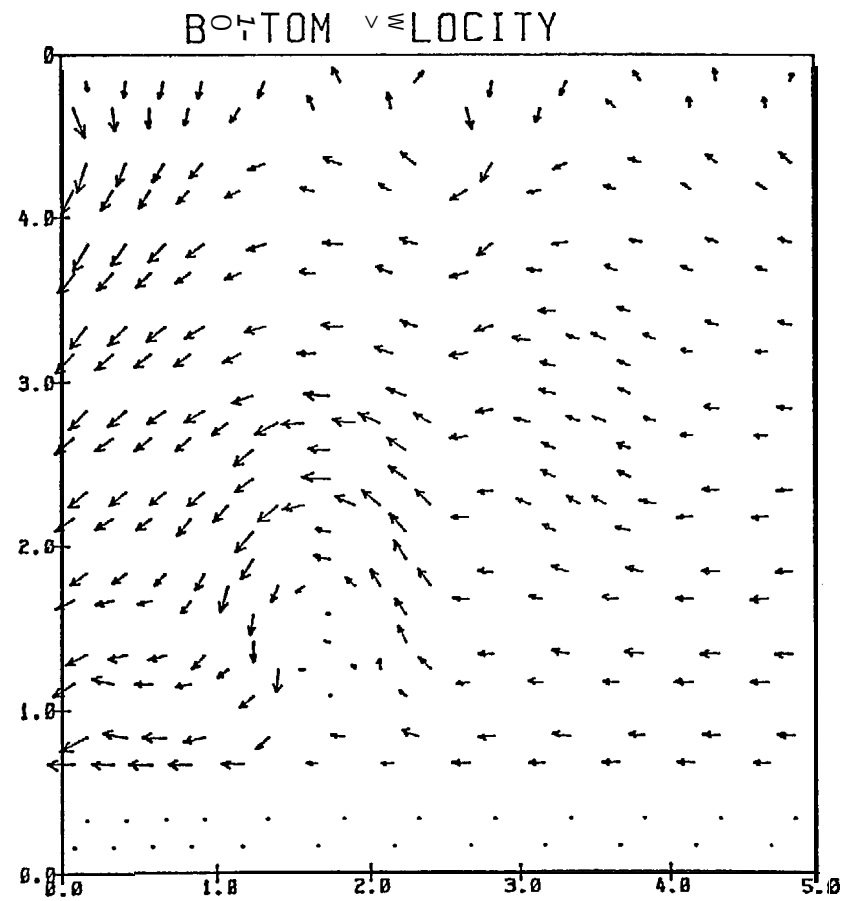


Figure 20c

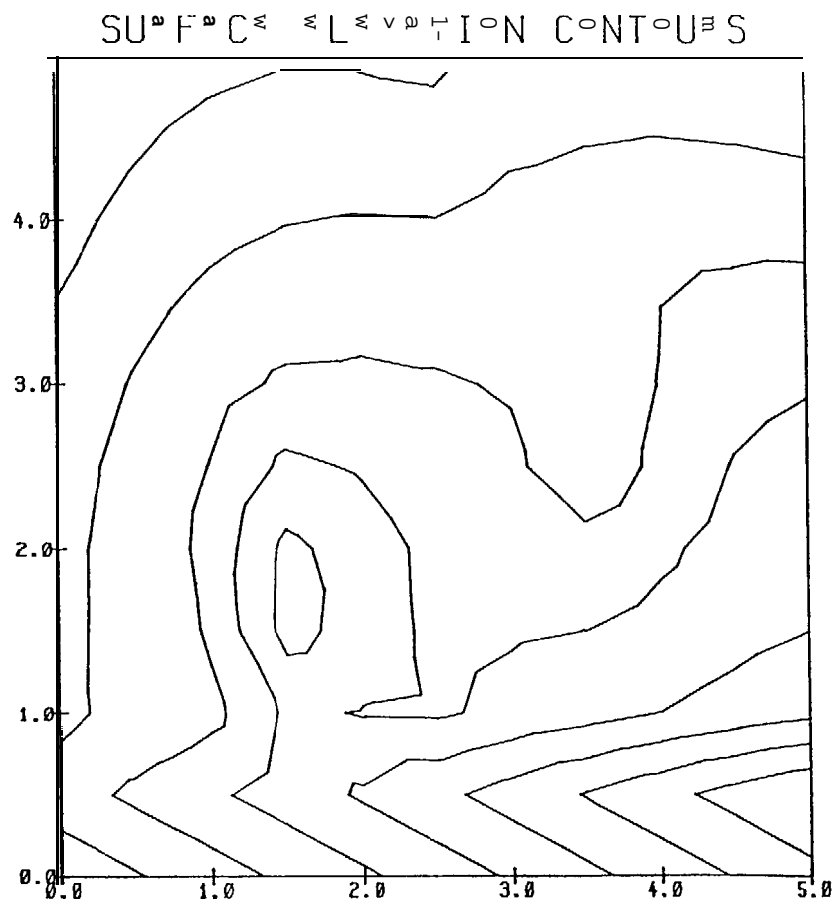


Figure 2 a

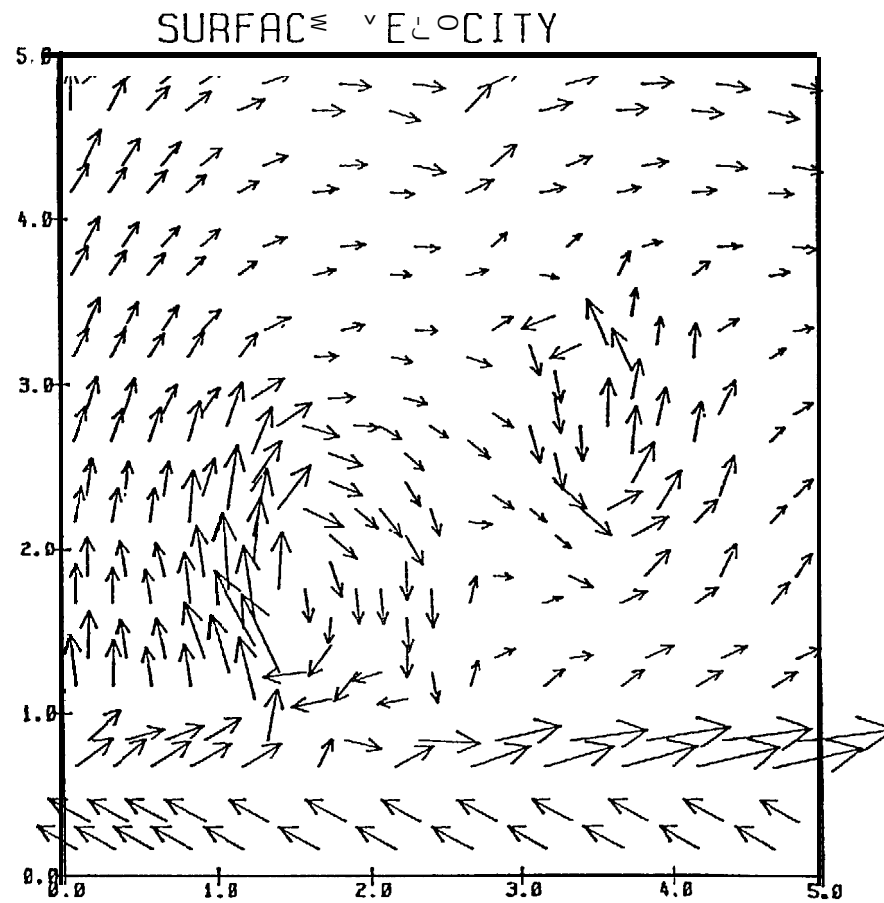


Figure 2 b

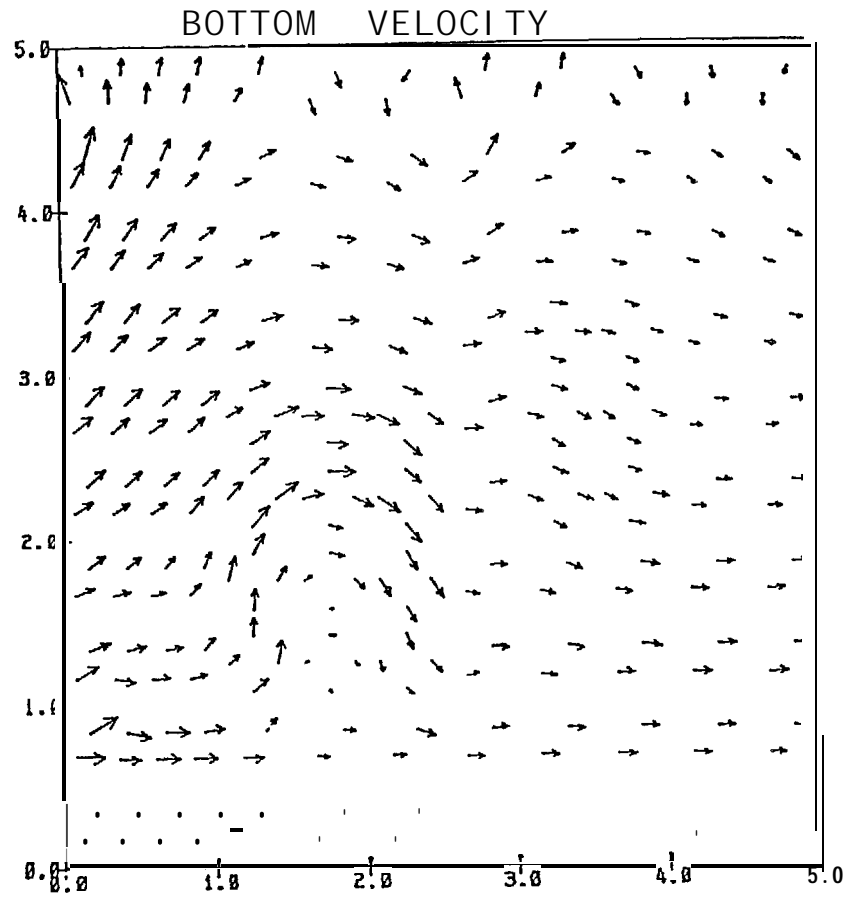


Figure 21c